

Physics of ultrathin films and heterostructures of rare earth nickelates

S. Middey,^{1,*} J. Chakhalian,^{1,†} P. Mahadevan,^{2,‡} J.

W. Freeland,^{3,§} A. J. Millis,^{4,¶} and D. D. Sarma^{5,**}

¹*Department of Physics, University of Arkansas, Fayetteville, Arkansas, USA, 72701*

²*S. N. Bose National Centre for Basic Sciences, Salt Lake, Kolkata, India, 700098*

³*Advanced Photon Source, Argonne National Laboratory, Argonne, Illinois, USA, 60439*

⁴*Department of Physics, Columbia University, New York, New York, USA, 10027*

⁵*Solid State and Structural Chemistry Unit,
Indian Institute of Science, Bangalore, India, 560012*

Abstract

The electronic structure of transition metal oxides featuring correlated electrons can be rationalized within the Zaanen-Sawatzky-Allen framework. Following a brief description of the present paradigms of electronic behavior, we focus on the physics of rare earth nickelates as an archetype of complexity emerging within the charge transfer regime. The intriguing prospect of realizing the physics of high T_c cuprates through heterostructuring resulted in a massive endeavor to epitaxially stabilize these materials in ultra-thin form. A plethora of new phenomena unfolded in such artificial structures due to the effect of epitaxial strain, quantum confinement, and interfacial charge transfer. Here we review the present status of artificial rare-earth nickelates in an effort to uncover the interconnection between the electronic and magnetic behavior and the underlying crystal structure. We conclude by discussing future directions to disentangle the puzzle regarding the origin of the metal-insulator transition, the role of oxygen holes, and the true nature of the antiferromagnetic spin configuration in the ultra-thin limit.

* smiddey@uark.edu

† jchakhal@uark.edu

‡ priya@bose.res.in

§ freeland@anl.gov

¶ millis@phys.columbia.edu

** sarma@sscu.iisc.ernet.in

I. INTRODUCTION

Complex oxides, consisting of transition metal ions offer a vast landscape of fascinating phenomena such as metal-insulator transitions, spin, charge and orbital orderings, high temperature superconductivity, colossal magnetoresistance and multiferroicity etc [1]. The subtle competition between the bandwidth (W), on-site electron-electron correlations (U), crystal structure and charge transfer energy between oxygen and transition metal sites (Δ), together with the possibility of multiple oxidation states typically available to transition metal ions and a wide range of structural variations results in an unprecedented diversity of interesting phenomena [2, 3]. The quest to understand and control these phenomena has captured the imagination of generations of condensed matter physicists and has fostered the development of advanced experimental probes and theoretical methods.

Thin films and heterostructures add an important new dimension to the problem. Recent advances in atomic precision oxide growth [4–8] enable new classes of materials to be created and studied. Behaviors exhibited by ultra-thin films and heterointerface systems are different than in bulk, and the multiplicity of options for film growth and heterostructuring open new possibilities for control of material form and thus, for controlled comparison of the relation between structure and properties. For example, growing films on different substrates lead to different strain states, and the materials respond with different degrees of octahedral tilts and rotations, resulting in different electronic properties. Similarly quantum confinement and interfacial charge transfer can change the underlying physics.

In this review, we focus on the perovskite rare earth nickelate compounds, with chemical formula $RENiO_3$ where $RE = \text{La, Pr, Nd, Sm, Eu} \dots \text{Lu}$. This material family exhibits rich physics including charge ordering, strong electron-lattice coupling, MIT and long period magnetically ordered state, all controlled by the interplay of crystal structure and electron correlations. Figure 1 schematically shows the rich diversity of ground state properties and their relationship to different physical parameters that can be controlled via diverse experimental realizations.

A crucial issue in the materials physics of complex oxides is orbital control. In a simple ionic picture, the Ni is in a low-spin d^7 state, with one electron in the two-fold degenerate e_g orbitals. In bulk materials, the occupation probabilities of the two orbitals are nearly equal. An issue that has attracted some recent interest is the extent to which “orbital engineering” (a controllable differential occupancy of the e_g orbitals by changing strain and quantum confinement in ultra-thin

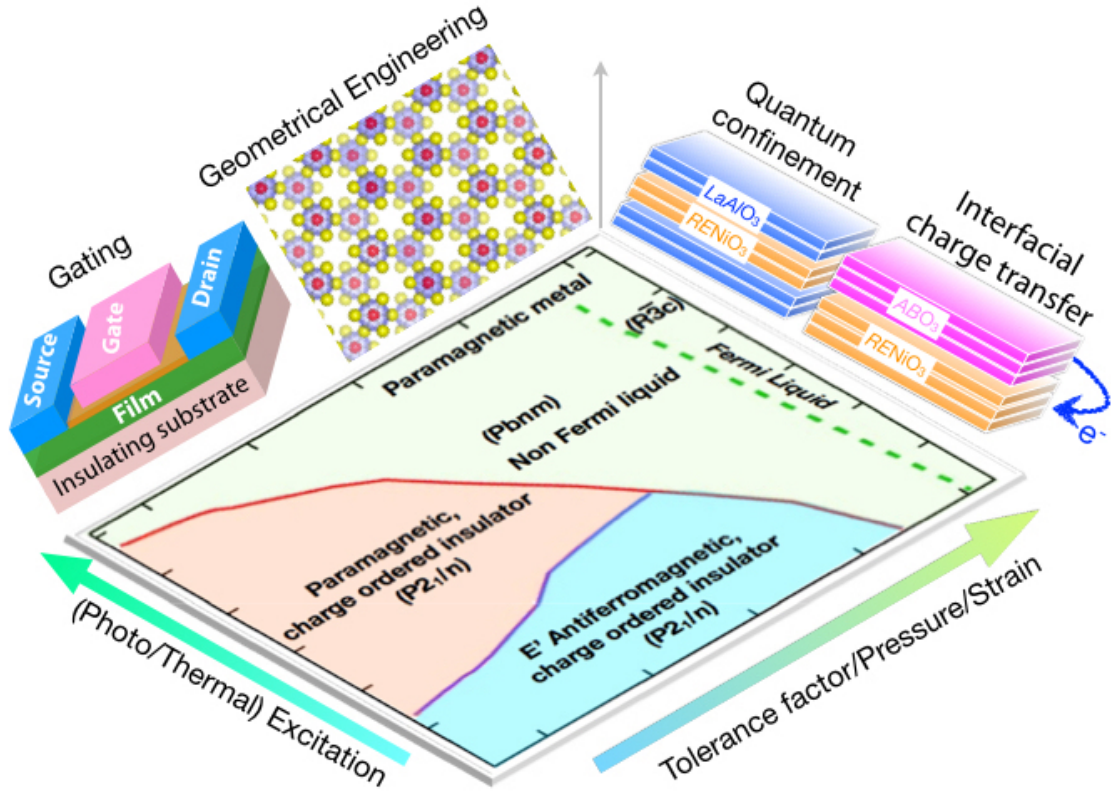


FIG. 1. Bulk phase diagram of $RENiO_3$ and various experimental ways of altering these ground states, discussed in this review.

films) is possible. The issue is important both in the context of the nickelate materials and more generally as an example of control of many-body electronic structure. In this article, we review the known properties of the bulk $RENiO_3$ materials and then how these are modified in ultra-thin film and heterostructured geometry.

II. CLASSIFICATION OF CORRELATED MATERIALS FROM AN ELECTRONIC STRUCTURE POINT OF VIEW

As these $RENiO_3$ are correlated oxides, we begin this review with a basic description of electronic structure parameters of such transition metal compounds. Efforts to classify the electronic structure of transition metal compounds started with attempts to understand why many of these have insulating ground states in spite of having partially filled d levels. Much attention has focused on NiO ; the notional electronic configuration of the Ni^{2+} ion is $3d^8$ in the crystal field split

$t_{2g}^6 e_g^2$ configuration, with fully filled t_{2g} -derived bands and half filled e_g -derived bands. One of the early suggestions due to Slater [9] emphasized the doubling of the unit cell due to the ground state antiferromagnetic order of NiO and the consequent opening of a gap in the half filled e_g bands. A density functional theory (DFT)-based *ab initio* band structure calculation [10] indeed obtained a ground state insulator for NiO. However, this approach is not entirely satisfactory, because the calculated band gap value is an order of magnitude smaller than the experimental value and NiO continues to show insulating behavior above the Néel temperature.

Mott [11, 12] proposed an alternative idea that strong correlation effects in the d -shell can lead to an insulating phase even in a system with partially occupied levels. Hubbard analyzed a theoretical model based on Mott's ideas and showed [13, 14] that a sufficiently large on-site Coulomb interaction strength, U , within a partially occupied level can indeed localize electrons. The one-electron removal spectrum, known as the lower Hubbard band (LHB) [corresponding to the occupied density of states (DOS) in a non-interacting system], is separated from the one-electron-addition spectrum, known as the upper Hubbard band (UHB) [corresponding to the unoccupied part of the DOS], shown in **Figure 2(a)**, when $U > U_c$, where U_c is in the order of the bandwidth (W) of the system dictated by the interatomic hopping interaction strength, t . Such a system known as the Mott-Hubbard insulator, and its band gap is controlled primarily by the magnitude of U .

Fujimori & Minami's [15] analysis of spectroscopic features of NiO established the additional necessity to account explicitly for oxygen $2p$ levels, since the primary hopping interaction t_{pd} in NiO connect O p and Ni d states. This requires the inclusion of an additional energy-scale, Δ , needed to transfer an electron from the fully-filled oxygen levels to a Ni $3d$ orbital. The presence of the O p band, arising from p - p hopping interactions between different oxygen sites, in a typical transition metal oxide is shown in **Figure 2(a)** for $\Delta > U$ limit. In the opposite limit of $\Delta < U$, the energy ordering of O p states, LHB, and UHB are as shown in **Figure 2(b)** for charge-transfer insulators [2], with the O p band appearing within the gap between UHB and LHB. In this limit, the band gap, measured between the top of the O p band and the bottom of the UHB, is controlled more by Δ than by U , in contrast to the case for Mott-Hubbard insulators (**Figure 2(a)**). This scenario forms the basis of the name, charge transfer insulator, as the lowest energy excitation for charge transport is achieved here by transferring an O p electron to the transition metal (TM) d orbital.

Combining these ideas, Zaanen, Sawatzky & Allen [2] suggested that, instead of a single U_c

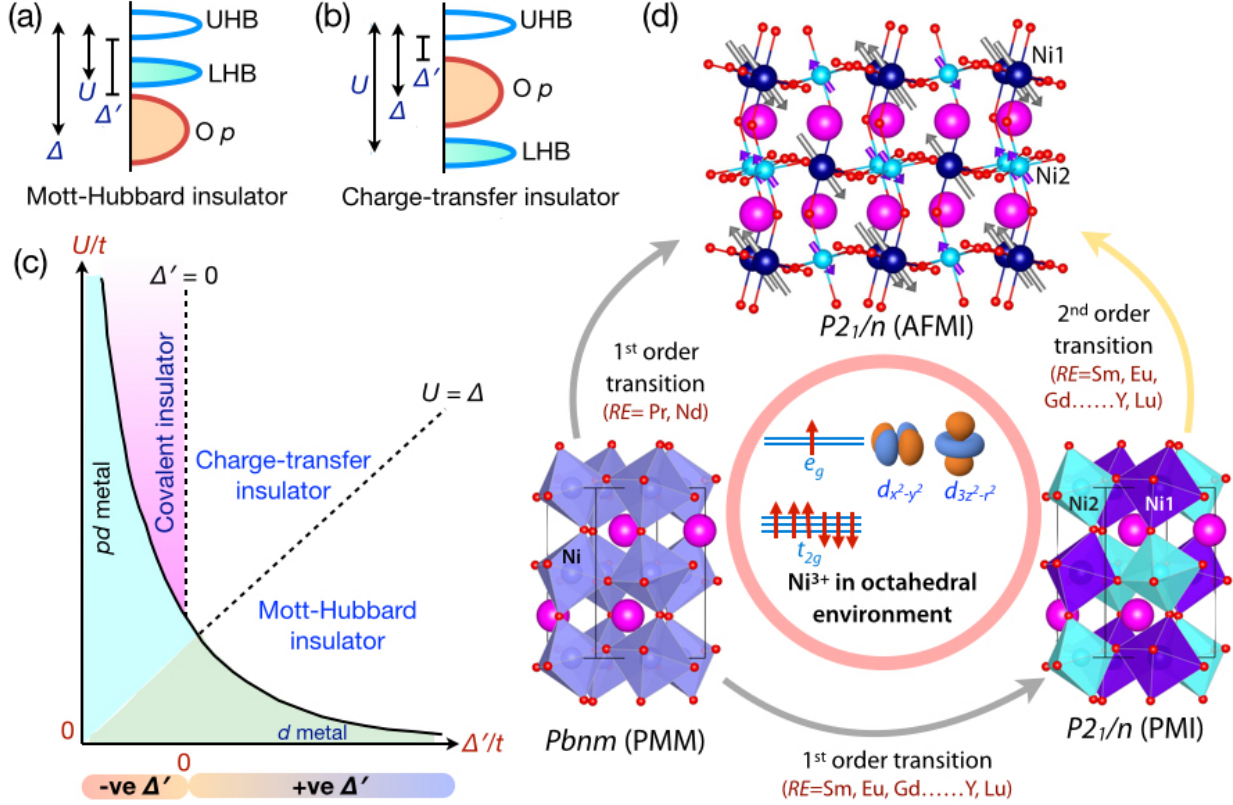


FIG. 2. (a, b) Schematics of energy levels for (a) Mott-Hubbard insulator, (b) charge-transfer insulator. (c) Modified Zaanen-Sawatzky-Allen phase diagram [2, 3]. (d) Various transitions observed in bulk $RENiO_3$ series depending on the choice of RE ion. The electronic configuration of a Ni^{3+} ion is also shown for a pure ionic picture (d^7).

as envisaged by Mott and Hubbard, the metallic and insulating ground states of transition metal compounds are separated by a line in the $U - \Delta$ phase space, with Mott-Hubbard insulators for $U_c < U < \Delta$ and charge transfer insulators for $U > \Delta > \Delta_c$. $3d$ orbitals contract across the $3d$ transition metal series, leading to a systematic increase in U [16]. Within a related series of oxides, it is also known [17] that Δ decreases across the Periodic Table due to rapid stabilization of the $3d$ level with the increasing atomic number. This approach broadly categorizes insulating oxides of early $3d$ transition metals as Mott-Hubbard type, with larger Δ and lower U , and those of late $3d$ transition metals as charge-transfer type, with smaller Δ and larger U .

For sufficiently small U , the system becomes metallic, as in the Mott's description of the insulator to metal transition, due to the overlap of the top of the LHB with the bottom of the UHB. Similarly, one would expect that for a small enough Δ that makes the top of the O p -band overlap

the bottom of the UHB, defining the zero of the *effective* charge transfer energy, Δ' (see **Figure 2(b)**), the system will become metallic, as also suggested in the original Zaanen-Sawatzky-Allen phase diagram [2]. However, it was later argued [18] that the insulating state will persist over a region of $\Delta' < 0$, depending on the value of t_{pd} and U , because t_{pd} will essentially mix the O p and metal d states, pushing them energetically apart to form a nonzero bandgap, similar to the case of bonding-antibonding splitting formed in molecular orbital theory. This new region in the $U - \Delta$ phase space was termed the covalent insulating regime [18] to stress that the band gap originated from the presence of a sizable t_{pd} mixing between O p and metal d -states or covalency. This regime has also been referred to in the literature as the negative Δ insulator [19, 20], though care should be taken in retaining the distinction between Δ and the *effective* charge transfer energy, Δ' , in this context. Explicit calculations [3, 21] showed that this covalent insulator regime is increasingly stabilized with increasing t_{pd} and U . **Figure 2(c)** shows the resulting phase diagram, indicating different insulating and metallic regimes and establishing that the late transition metal oxides that are close to MITS, for example, many interesting Ni and Cu compounds, including the nickelates discussed in this review, belong to the covalent regime in their insulating state. Increasing the formal valence of a transition metal ion has the primary effect of lowering Δ and increasing t_{pd} . Thus, compounds of earlier transition metals, such as Co, Fe, Mn and even Cr may also be in the covalent insulating regime in their higher valence states. The correlation physics is different within the covalent insulating regime from the standard Mott paradigm due to the effective charge transfer energy being negative. One of the direct consequences of this negative effective charge transfer energy is that the ground state wave function has a significant and often dominant contribution from the $d^{n+1}\underline{L}$ state, where n is the nominal d electron count and \underline{L} denotes a hole state generated in the ligand p orbitals; this is in contrast to the Mott limit where the dominant contribution arise from d^n states. In the case of nickelates, with a formal d^7 configuration of Ni^{3+} , this ensures a significant contribution of the $d^8\underline{L}$ state in the ground-state wave function as the expense of the contribution from d^7 states.

The above discussion suggests that localizing effects of increasing U and Δ are obviously important; however, the delocalizing effects arising from various hopping interactions as well as any other interaction such as the crystal field and the spin-orbit interaction, that may influence the bandwidth are also important and need to be treated on equal footing. This objective has been most successfully achieved through extensive developments of Dynamical Mean Field Theory (DMFT), which provides the basis of most of our discussion of the electronic structure of nickelates in later

sections of this review. At a simpler level of broad classifications, we already know from experimental studies that LaNiO_3 (LNO) is metallic, whereas all other members of the series, $RE\text{NiO}_3$, where RE is a rare-earth ion, are insulators at low temperature. Ab-initio electronic structure calculations for the series $RE\text{NiO}_3$ ($RE=\text{La, Pr, Nd, Sm}$ and Ho) [22] established a systematic reduction in the Ni d -bandwidth by approximately 10% between La and Ho compounds. A fitting of the ab-initio band dispersions to a minimal tight-binding model with Ni d and O p states, did not show any substantial variation of t_{pd} across the series. The bandwidth reduction can, therefore, be related to the reduction of the hopping between different NiO_6 octahedra driven by a decreasing interoctahedral Ni-O-Ni angle with smaller RE ions across the series. Various features in the valence band photoemission spectra of LaNiO_3 and NdNiO_3 (NNO) could be identified with features in the calculated density of states, underlining the importance of band structure effects [23, 24]. An analysis of the $L_{23}M_{45}M_{45}$ Ni Auger spectrum revealed U of Ni to be 4.7 ± 0.5 eV. Hartree-Fock type mean-field solutions of a multiband Hubbard model with these parameter strengths were found [23] to be consistent with LNO being metallic and NNO insulating.

III. COMPLEXITY IN BULK $RENIO_3$

Although we begin our discussion of ultra-thin film nickelates by briefly reviewing several key phenomena present in the bulk counterpart, we refer the reader to the reviews by Medarde [25] and Catalan [26] these reviews for more details concerning bulk properties. Whereas the first member of the nickelate series, LaNiO_3 with rhombohedral $R\bar{3}c$ structure remains metallic down to the lowest temperature probed, the intermediate members with $RE = \text{Pr}$ and Nd undergo a first-order MIT from the paramagnetic metallic (PMM) state with orthorhombic ($Pbnm$) structure to an antiferromagnetic insulating (AFI) state accompanied with a lowering of symmetry to monoclinic ($P2_1/n$). As the tolerance factor ($t = d_{RE-O}/\sqrt{2}d_{Ni-O}$; where d_{RE-O} and d_{Ni-O} are ionic bond distances between RE and O and between Ni and O respectively) decreases further away from unity for even smaller RE ions (e.g. Sm...Lu), the MIT temperature (T_{MIT}) and magnetic transition (T_N) start to separate from each other (**Figure 1**). Within the insulating phase, the entire family has monoclinic ($P2_1/n$) structure (**Figure 1 and 2(c)**) with two inequivalent Ni sites in the unit cell.

Electrical and thermal measurements on the bulk and thin films revealed the signatures of complex multi-band behavior [27], which has been further corroborated by angle resolved photoemission spectroscopy (ARPES) measurement [28]. Surprisingly, despite sharp changes in conduc-

tivity and lattice parameters across the MIT, optical conductivity measurements revealed only a gradual opening of band gap with continuous changes in spectral weight of the Drude peak [29]. The reported optical gap of ~ 1 eV is also much larger than the gap (~ 20 meV) obtained from electrical conductivity data [30]. Recent tunneling experiment showed the opening of a sharp gap (~ 30 meV) in the insulating state and also the existence of pseudo gap in metallic LaNiO_3 [31].

In the ionic picture, $RENiO_3$ compounds have NiO_6 octahedra with Ni^{3+} ions in the d^7 low-spin electronic configuration ($t_{2g}^6 e_g^1 : S = 1/2$), which are expected to be Jahn-Teller active. However, resonant X-ray diffraction (RXD) experiments showed ordering of local magnetic moments on Ni sites in AFI phase and ruled out any orbital ordering [32, 33]. The magnetic ground state of these spins (**Figure 2(c)**) was initially deduced from neutron powder diffraction (NPD) [34]. The magnetic wave vector for the antiferromagnetic state was determined to be $(1/2, 0, 1/2)_{\text{ortho}}$ [$(1/4, 1/4, 1/4)$ in pseudo cubic notation]; the spin arrangement of this E' -AFM state can be viewed as either a sequence of $\uparrow\uparrow\downarrow\downarrow$ or $\uparrow \rightarrow \downarrow \leftarrow$ pseudo-cubic $(1\ 1\ 1)$ planes and the non-collinear spin scenario has been demonstrated by resonant x-ray scattering [35]. Whereas two distinct magnetic moments $1.4 \mu_B$ and $0.7 \mu_B$ consistent with a checker board type charge ordering pattern were determined for YNiO_3 [36], the magnetic moments in the $RE = \text{Pr}$ [34, 37], Nd [34, 37], Sm [37, 38], Eu [37, 38] compounds were found to be similar on each Ni site. This surprising result was further corroborated by RXD experiments, in which a very similar energy dependence of magnetic scattering intensity was recorded across the series, with an similar spectroscopic signature for the local moment on Ni [39]. In view of the strong variation of structural distortion and the magnitude of T_{MIT} in the $RENiO_3$ series, both measurements raised concern about the true nature of the charge ordering state. A view which aligns many of these facts is the picture where the strong covalency leads to the ground state to be more $3d^8 \underline{L}$, and the charge ordering pattern in this picture resides not on Ni but on the oxygen site (i.e. $3d^8 \underline{L} - 3d^8 \underline{L} \rightarrow 3d^8 - 3d^8 \underline{L}^2$) [40].

IV. EPITAXIAL STABILIZATION

The +2 charge state is the most common oxidation state of Ni and the $RENiO_3$ requires Ni oxidation state to be +3. Such high oxidation state is stabilized only under a high oxygen pressure $P \sim 200$ bar, and an elevated temperature of 1000°C [41]. Despite the extreme synthesis conditions, to-date only micrometer-sized single crystals have been obtained for these nickelates (except for LNO) [42], limiting the application of many experimental techniques crucial for understanding

the underlying physics of these materials. As an alternate route, the growth of thin films is a feasible solution for obtaining large-size single-crystalline materials. Not surprisingly, many crucial pieces of information discussed in the last section were obtained by using single-crystalline thin films.

A. Thermodynamic Stability:

Whereas thin films of LNO could be grown without high oxygen pressure by pulsed laser deposition (PLD) [43] and sputtering [44], stoichiometric NdNiO₃ films with a bulk-like MIT were initially achieved only by postannealing under a high oxygen pressure (~ 115 bar) [45]. Later, epitaxial films for several members of the family were successfully synthesized at much reduced oxygen pressure (< 0.02 bar) by metal-organic chemical vapor deposition (MOCVD) techniques by Novojilov et al. [46]. Following this success, the high quality epitaxy at low oxygen partial pressure has been also realized by PLD [47], sputtering [48] and all-oxide molecular beam epitaxy (MBE) [49].

To understand how a single crystalline phase can be obtained outside the thermodynamic phase diagram [$P(O_2)$ - T] of bulk materials, we consider the model of epitaxial stabilization of thin films [50]. In this phenomenological framework, the relative difference between the free energies for the bulk and epitaxially stabilized phases is given by:

$$\Delta E = \Delta E^{ic} - \Delta E^c = h[\Delta g_v^{ic} - \Delta g_v^c - \frac{\mu}{1-\nu}\epsilon^2] + [\sigma_s^{ic} - \sigma_s^c] \quad (1)$$

Here the superscripts c and ic denote the epitaxially coherent and incoherent (i.e. free from substrate) phases, respectively, h is the film thickness, Δg_v is the Gibbs free energy per unit volume, μ is the shear modulus, ν is a Poisson's ratio, ϵ is the relative lattice mismatch between the unit cell parameters of the desired phase and the substrate and σ_s is the surface tension. Whereas the volume contribution (the first term) is always negative, the surface contribution (the second term) is always positive. If the energy contributions are such that $\Delta E > 0$, then an epitaxially coherent phase is stabilized [50]. As seen in equation 1, a dramatic reduction in the contribution to the free energy comes from the coherent film-substrate interface, implying that $RENiO_3$ phases can be stabilized on a perovskite substrate whereas the films on non-perovskite substrates like MgO and ZrO₂ lack the required coherency and enforce the phase decomposition to $RENiO_3 \rightarrow REO_x + NiO$ [51]. Moreover, as indicated by equation (1), the increase of film thickness (h) as well

as the larger lattice mismatch (ϵ) may further amplify the phase decomposition (i.e. RE_2O_3 and NiO) away from the single phase perovskite film [46]. Because the formation energy of $RENiO_3$ [$\Delta G_{RENiO_3} = \Delta G_{LaNiO_3} + (h - sT)(r_{RE^{3+}} - r_{La^{3+}} - \frac{1}{4}RT \ln(P))$] also increases with a decreasing tolerance factor [52], the epitaxial stabilization of the distorted members of the series becomes much more difficult. In recent years, several groups have overcome this challenge and have successfully stabilized ultra-thin films of $RENiO_3$ with $RE = Pr, Nd, Sm$ and Eu [53–59].

B. Polarity mismatch:

The interest in nickelate heterostructures also brought to light the issue of polar discontinuity at the substrate-film interface that results in a diverging potential, which is compensated in several ways, e.g. by electronic reconstruction, cationic inter-mixing or oxygen vacancies [60]. In a pure ionic model, because $RENiO_3$ consists of alternating $[REO]^{1+}$, $[NiO_2]^{1-}$ atomic planes along the pseudo cubic (0 0 1) direction, this polarity issue was investigated by growing a [1 uc LNO/1 uc LAO] superlattice on non-polar STO ($[SrO]^0$, $[TiO_2]^0$) and polar LAO ($[LaO]^{1+}$, $[AlO_2]^{1-}$) (uc denotes pseudocubic unit cell). Whereas the matched polarity on the LAO substrate yields the desired +3 valence of Ni, the polar mismatched case of LNO on STO yields the first unit cell with Ni in the +2 oxidation state [61]. Careful high-resolution transmission electron microscopy (HRTEM) combined with electron energy loss spectroscopy (EELS) confirmed $Ni^{2+}O^{2-}$ precipitation driven by the interfacial polar fields [62]. This precipitation of the Ni^{2+} containing layer can be suppressed by the careful growth of a buffer layer of LAO, which allows for the preservation of Ni^{3+} [61] in all nickel containing layers. These experiments highlight the importance of taking into account the polarity mismatch in understanding material properties in heterostructures.

V. GROUND STATE ENGINEERING THROUGH HETEROEPITAXY

Epitaxial stabilization on such perovskite substrate not only provides the desired single crystalline materials, but also allows ground state engineering of nickelates by implementing the effect of strain, confinement, charge transfer etc. The rapid progresses along these directions of research in recent times have been discussed in this section.

A. Epitaxial strain in ultra thin films

Because epitaxial growth on a single-crystalline substrate forces the film to have the same in-plane lattice parameters during the atom-on-atom growth; distortions, lattice symmetry, octahedral tilts and rotations in the resulting thin film may become quite different from the bulk counterpart [63]. Epitaxial strain is conventionally quantified by $\epsilon = (a_{\text{bulk}} - a_{\text{sub}})/a_{\text{bulk}}$, where a_{bulk} and a_{sub} are the pseudo cubic lattice constants of bulk $RENiO_3$ and the substrate, respectively. However, as some chemical nonstoichiometry may be introduced during the growth, actual ϵ should be calculated using the experimentally measured lattice constant of an unstrained film (instead of a_{bulk}). The effect of strain on electronic and magnetic transitions of $RENiO_3$ series has been thoroughly explored by diverse experimental probes including thermal measurements and Hall effect measurement [58, 64, 65], synchrotron X-ray diffraction [66, 67], X-ray absorption spectroscopy [67–71], resonant soft X-ray scattering [69, 72, 73], ARPES [74, 75], optical spectroscopy [72, 76–78].

1. Orbital response to heteroepitaxy

Magnetic interactions in transition metal oxides are determined by the specific geometry of chemical bonds, the presence of various pathways for exchange interactions, the orbital configuration of the transition metal ions, and d electron occupancy. The strength and the nature (ferro- vs. anti-ferromagnetic) of these exchange interactions can be summarized by the set of phenomenological rules, collectively known as Goodenough-Kanamori-Anderson rules, that reflect the strong intercoupling between spin, charge and orbital degrees of freedom. On this basis, the fundamental step to employing heteroepitaxial engineering is to alter via the orbital-lattice interactions, the d -band orbital occupation and energy level splittings caused by biaxial strain induced lattice deformations. The orbital engineering in nickelates can be rationalized in the following way: coherent heteroepitaxy imposes a tetragonal distortion on the film, thus removing the twofold e_g orbital degeneracy due to the distortion of octahedral ligand field. Because both $d_{x^2-y^2}$ and $d_{3z^2-r^2}$ orbitals, constituting the degenerate e_g orbitals in an octahedral crystal field, have even symmetry, both tensile and compressive strains should symmetrically alter their energy positions relative to the strain-free energy band center. Although this symmetric strain-induced orbital polarization (SIOP) (**Figure 3(a)**) concept is a common view for rationalizing orbital responses, surprisingly,

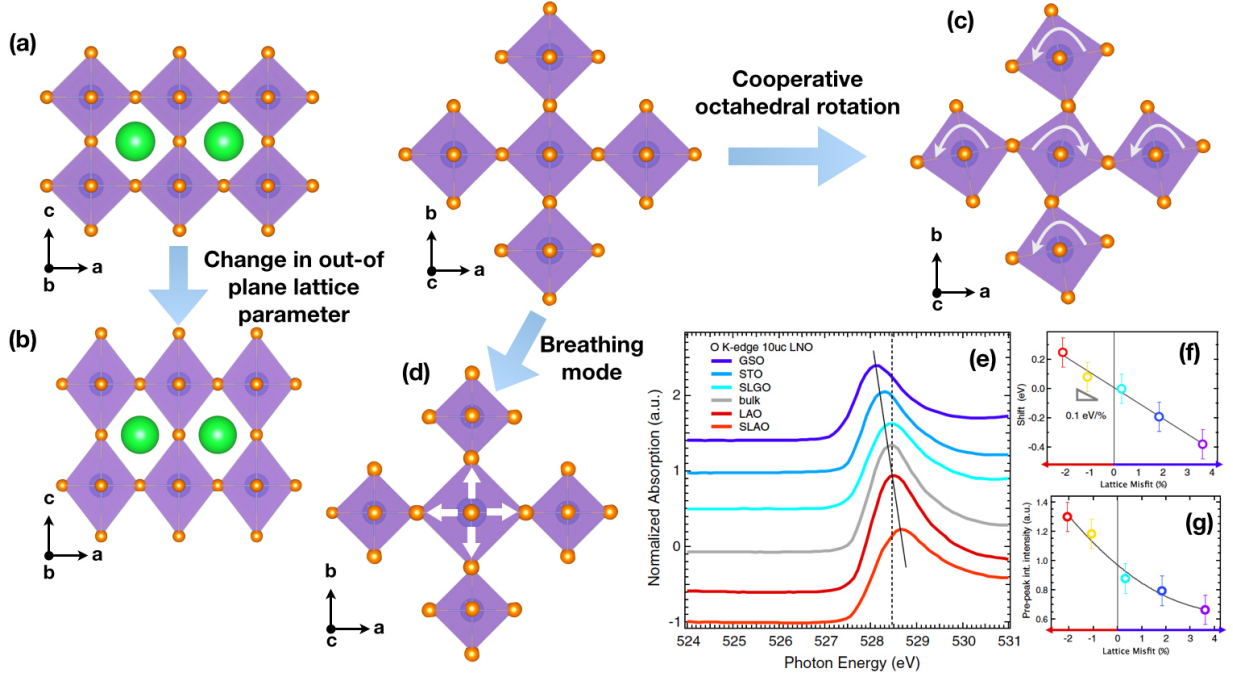


FIG. 3. (a)-(d) Different types of distortions for accommodating lattice mismatch. (b) Out of plane expansion in an octahedron in accordance with the concept of symmetric strain-induced orbital polarization. (c) Cooperative octahedral rotation. (d) Breathing mode. (e)-(g) Effect of strain-induced change in Ni-O covalency for LNO. (e) Pre-peak in O K -edge absorption for various strain states. Variation in (f) peak position and (g) normalized full width at half-maximum relative to bulk LNO with misfit ϵ . Abbreviations: LAO, LaAlO₃; STO, SrTiO₃; GSO, GdScO₃; SLGO, SrLaGaO₄; SLAO, SrLaAlO₄. Reprinted (panel (e)-(g)) with permission from Reference [68] [J. Chakhalian et al., Phys. Rev. Lett. **107**, 116805 (2011).] Copyright (2011) by the American Physical Society.

ultra thin films of many perovskite oxides surprisingly do not follow this simple notion [79].

To understand how the SIOP model is violated, a 10 uc thick film of LaNiO₃ (LNO) was grown on LAO ($\epsilon = -1.1\%$) and STO ($\epsilon = +1.8\%$) substrates [68]. For the LAO case, X-ray linear dichroism (XLD) measurement showed a 100 meV lowering of the Ni $d_{3z^2-r^2}$ orbital compared to the $d_{x^2-y^2}$ orbital, confirming the compression of in-plane Ni-O bonds and enlargement of the out-of-plane (apical) Ni-O bonds, as expected from the SIOP model. Following the SIOP model, an inversion of the e_g orbitals was expected for tensile strain on STO. Surprisingly, no orbital polarization was detected for the STO case, although reciprocal space mapping confirmed that the film was fully coherent with in-plane lattice matched to the STO substrate [67, 68]. This asymmetric orbital-lattice response to epitaxial strain signals the existence of alternative compensation

mechanisms for strain accommodation [63, 80]. Density functional theory (DFT) calculations with the experimentally determined lattice constants showed the existence of single type NiO₆ octahedra with different in-plane and out-of-plane Ni-O bonds resulting in finite orbital polarization for compressive strain. In contrast, tensile strain was preferentially accommodated by cooperative octahedral rotations (**Figure 3(b)**) and breathing mode distortions (**Figure 3(c)**). The importance of these phonon modes is highlighted by the observation of breathing mode distortion, that causes a Ni-O bond-length disproportionation with alternating octahedra of Ni(1)O₆ (short Ni-O bonds) and Ni(2)O₆ (long Ni-O bonds), which are all equivalent in the bulk LNO.

Further XLD experiments on NNO films revealed that contrary to LNO, under tensile strain the $d_{3z^2-r^2}$ orbital has a higher energy compared to the $d_{x^2-y^2}$ [67], as expected from the SIOP model for tensile strain. Such lifting of orbital degeneracy was also seen by hard X-ray RIXS (resonant inelastic X-ray scattering) measurements, that identified a splitting of 0.4 eV between the e_g states [81]. This markedly different response of LNO vs. NNO was attributed to the difference in octahedral rotational pattern of bulk: $a^- a^- a^-$ (LNO) and $a^- a^- c^+$ (NNO) in Glazer notation, thus emphasizing the importance of lattice symmetry and how it interacts with strain driven distortions of the structure [67].

2. Strain induced self-doping

Because $RENiO_3$ belong to a part of U - Δ phase space with an effectively negative charge transfer energy and a high degree of covalency, the ground state of $RENiO_3$ is a strong admixture of d^7 and $d^8 \underline{L}$ electronic configurations (\underline{L} is a ligand hole on the oxygen p orbitals). This $d^8 \underline{L}$ state manifests itself as a characteristic pre-peak around 528.5 eV in O K edge ($1s \rightarrow p$) X-ray absorption spectra (XAS). Due to the weak core-hole interaction, the O K edge XAS is an approximate measure of oxygen projected unoccupied density of states [82], and the intensity, position, and width of the pre-peak are the markers of the degree of Ni-O bond covalency. As shown in **Figure 3(e)**, for the series of LNO films subjected to both tensile and compressive strain, the pre-peak revealed a systematic evolution in the peak energy position with the imposed amount of epitaxial strain. The direct strain control of ligand-hole density was deduced from the nearly linear dependence of the peak position with ϵ , **Figure 3(f)**. The charge transfer energy (Δ ($= e \delta V_{\text{Mad}} + I(\text{O}^{2-}) - A(\text{M}^{\nu+}) - e^2/d_{\text{M-O}}$ in the ionic model [1], where $I(\text{O}^{2-})$ is the ionization potential of oxygen, $A(\text{M}^{\nu+})$ is the electron affinity of transition metal ion $\text{M}^{\nu+}$ ion and $d_{\text{M-O}}$ is the nearest

neighbor metal-oxygen distance) depends on the relative Madelung potential δV_{Mad} between Ni and O, so the movement of the prepeak highlights a decrease in Δ with compressive strain. The corresponding decrease in full width at half maximum (FWHM) with increasing tensile strain **Figure 3(g)** implies the narrowing of electron bandwidth (W). The strong modulation in both Δ and W implies a strain-induced unusual self-doping effect, which was further substantiated by temperature-dependent Hall coefficient and thermoelectric power measurements [65].

3. Strain driven phase engineering

As the nature of the ground states and the transition temperatures depend strongly of Ni-O-Ni bond angle and Ni-O bond length, epitaxial strain is expected to have a profound impact on the electronic and magnetic properties. To investigate this possibility, Liu et al., [56, 69] investigated 6 nm NNO films as a function of epitaxial strain. The result shown in **Figure 4(a)** indicates that unlike the bulk where $T_{\text{MIT}} = T_N$, the transitions get separated, with the degree of separation scaling with tensile strain. On the compressive side, the temperature-induced MIT is completely quenched. Although several reports [46, 83–85] revealed the preservation of the MIT in compressively strained films, a recent study by Hauser et al. [58] demonstrated that those films are actually partially relaxed, and optimally prepared films under compressive strain are entirely metallic [58, 86], consistent with the report of Liu and coworkers [56, 69]. These studies found the resistivity of this anomalous metallic state exhibits non-Fermi liquid (NFL) behavior in the vicinity of a quantum critical point akin to the case of bulk PrNiO_3 under external pressure [87, 88]. From those observations, it was concluded that film behavior under increasing tensile strain resembles the A -site replacement by a smaller RE ion of the bulk, whereas the effect of compressive strain is very similar to that of hydrostatic pressure. The exponent of NFL phase is also not affected by the change of film thickness [86]. Although resistance of these films surpasses the Mott-Ioffe-Regel limit at high temperature [89], unlike the case for the cuprates ρ eventually saturates for nickelates. This behavior was shown to related with the orbital splitting between $d_{x^2-y^2}$ and $d_{3z^2-r^2}$ orbitals [86]. . The effect of epitaxial strain was also investigated for the distorted $RENiO_3$ members with $T_{\text{MIT}} > T_N$ [70, 71, 73]. Similar to the NNO case, the separation between T_{MIT} and T_N decreases as the amount of tensile strain is lowered and the films grown under large compressive strain becomes entirely metallic [73].

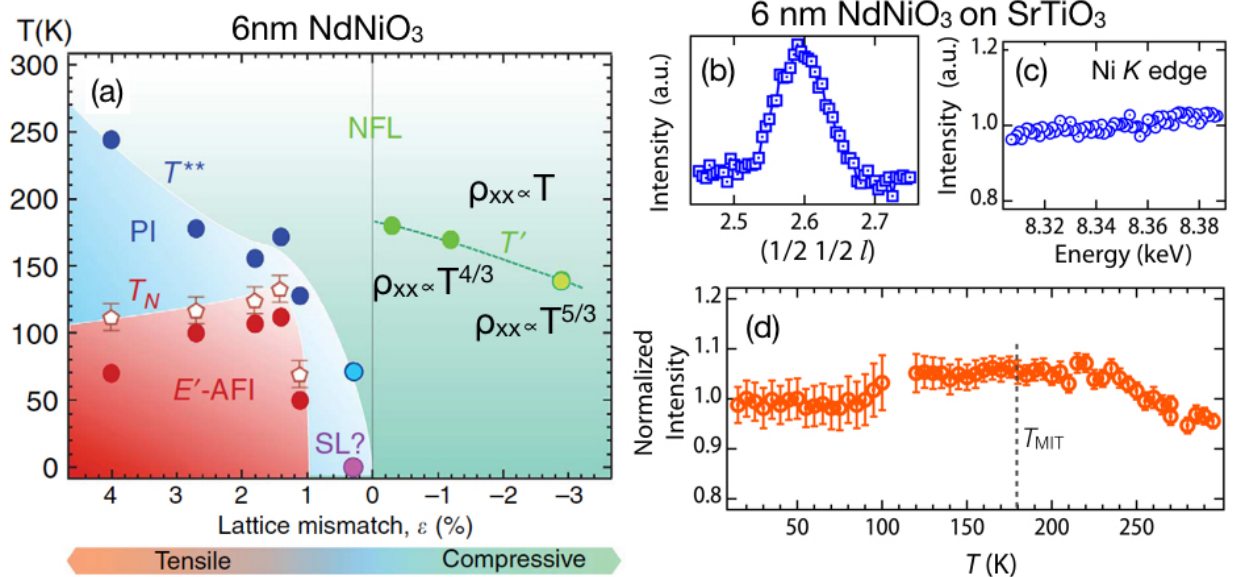


FIG. 4. (a) Lattice mismatch-temperature phase diagram for 6 nm thin NNO film. Panel (a) adapted from Reference [69] NFL, PI and AFI denote non-Fermi liquid, paramagnetic insulator and AFM insulator, respectively. T^{**} (blue), T_0 (green) and the hysteric inflection point (red) are denoted by closed circles, whereas T_N is denoted by open pentagon and its error bar is defined as the temperature step size, 10 K. (b) l scan through $(1/2\ 1/2\ 5/2)_{pc}$ reflection for NNO on STO substrate. Due to the twinned domain structure of the film, this reflection is a combination of $(105)_{ortho}$, $(015)_{ortho}$, $(231)_{ortho}$, $(321)_{ortho}$ reflections. (c) Ni does not contribute to this reflection even in the insulating phase as demonstrated by the energy scan around the Ni K -edge. (d) Temperature dependence of this reflection, recorded during the heating run from low temperature. For details of panels (b)-(d), see Reference [81]. The absence of Ni contribution to the $(h\ 0\ l)_{ortho}$ reflection with odd h and l in such ultrathin films was also confirmed for single-domain NNO film, grown on a NdGaO_3 substrate [90].

4. Selective suppression of order parameters through epitaxy

Although both the antiferromagnetic order and the MIT are preserved in epitaxially grown NNO films with $\epsilon > +1.1\%$, the next important question is whether the proximity to the substrate of different crystal symmetry can alter the orthorhombic to monoclinic symmetry lowering across the MIT and the concomitant charge ordering. The charge ordering scenario in the bulk-like NNO films was investigated with resonant X-ray scattering experiments at the Ni K -edge [91]. In the high-symmetry orthorhombic metallic phase Ni sites do not contribute to particular reflections,

which gain a Ni contribution in the low temperature monoclinic phase and can be used to study the details of the charge ordering phase via the resonant signature [32, 91, 92]. An interesting recent result is that, for an ultrathin (6 nm) NdNiO₃ film grown under tensile strain, even though the film displayed an MIT and magnetic ordering, there was no resonant Ni signal for these reflections even in the insulating phase (**Figure 4(c)**). This observation, together with the absence of any detectable temperature dependence of the reflection (**Figure 4(d)**), led to the conclusion that *Pbnm* symmetry is preserved deep into the insulating state [81, 90]. This result implies the exceptionally rare case of a purely electronic Mott-Hubbard MIT that is driven by the magnetic ordering.

Despite the absence of both the lattice symmetry change and Ni charge disproportionation, the transition was found to be accompanied by a peculiar charge redistribution from the Ni 3*d* to Nd 5*d* orbitals that may play a role in the MIT [81]. Although the relevance of Mott-Hubbard picture about the nature of the MIT was highlighted by the mid-gap spectral weight transfer in optics measurements [76], the charge redistribution which involves the *A*-site states questions the simple picture of the conventional Mott transition. The *K*-edge RIXS measurement and the resonant x-ray scattering data suggest that the MIT is neither pure Mott-Hubbard nor charge-transfer.

In contrast to the case for NdNiO₃, the bulk-like charge ordering pattern remains unaltered in ultra-thin films of highly distorted EuNiO₃ [93]. Those experiments stress the exquisite sensitivity of the electronic structure in the insulating state to various type of structural distortions [94] including the Jahn-Teller distortion (NdNiO₃) and breathing mode distortion (EuNiO₃), under epitaxial constraint. The issue of charge ordering in such geometry was also investigated by Raman scattering [72], and phonon modes characteristic of the charge ordering were indeed observed in insulating state of thin film and superlattices of PrNiO₃ (of thickness ~ 12 nm) under tensile strain. Interestingly, these Raman modes were absent in superlattices under compressive strain, which are weakly metallic but retain *E'* antiferromagnetic ordering. Such an antiferromagnetic, metallic phase does not exist in the bulk nickelate and has been referred to as a spin-density wave phase [72], which was predicted theoretically by Lee and co-workers [95, 96].

B. Quantum confinement in heterostructures

The ability to grow these materials with sub-unit cell precision has opened another new dimension to explore highly two-dimensional electronic and magnetic phases in the quantum confinement regime. The SL structure consisting of an electronically active material and a wide band

gap insulator (one side can be vacuum) blocks electron hopping along the confining direction (i.e. across the interface), the specific choice of confining interface further determines the boundary condition in this quantum well geometry. In this section, we explore how heterostructures can be used to tune the electronic and magnetic states of nickelates.

1. Dimensionality and Carrier Localization

The correlated metallic behavior of bulk LNO provides a perfect play ground to test the itinerant behavior of d -electrons down to the atomic scale. Toward this goal, several groups explored the effect of dimensionality along with electron-electron correlations was explored by growing a series of single layer films and SL structures of LNO of different thicknesses [48, 75, 97–101]. As an example, consider the results in **Figure 5(a)**, showing the temperature dependent resistivity behavior for a series of LNO films grown on LAO substrates by oxide molecular beam epitaxy [75]. Although the room temperature conductivity decreases with decreasing film thickness, the metallicity over the entire temperature range is maintained down to 4 uc. Upon approaching the 2 uc limit, the LNO film becomes insulating. Although all groups have reported this confinement induced MIT, the critical film thickness at which the insulating behavior sets in is strongly dependent on the strain value and the architecture (i.e. film vs. SL). With respect to dimensionality effects in single layer films, one issue is the presence (or lack) of a polar discontinuity, which may explain the differences between the results on LAO [75] vs. STO [97]. Resonant X-ray absorption spectroscopic measurements on Ni $L_{3,2}$ -edge complemented by first principle calculation [98] and soft, hard X-ray photoemission spectroscopic measurements [100, 102] revealed a gradual evolution of electronic structure including the charge transfer gap. X-ray diffraction showed a change in atomic arrangement, in terms of both decreased Ni-O-Ni bond angle and lattice rumpling near the interface with a reduced number of unit cells [101]. In addition, layer-resolved studies established that the suppression of DOS is more pronounced near the interface [103], where the octahedral tilts are larger than in layers away from the interface [101, 104]. All of these results indicate that the bandwidth control is an important component for the MIT as is the case for bulk nickelates [25, 26].

Recent ARPES studies [75] revealed the retention of bulk-like electronic structure and Fermi liquid characteristics (see narrow parabolic band in **(Figure 5(b)-(d))**) down to 3 u.c. thin film and the thickness dependent MIT was attributed to the presence of a spin/charge instability in two

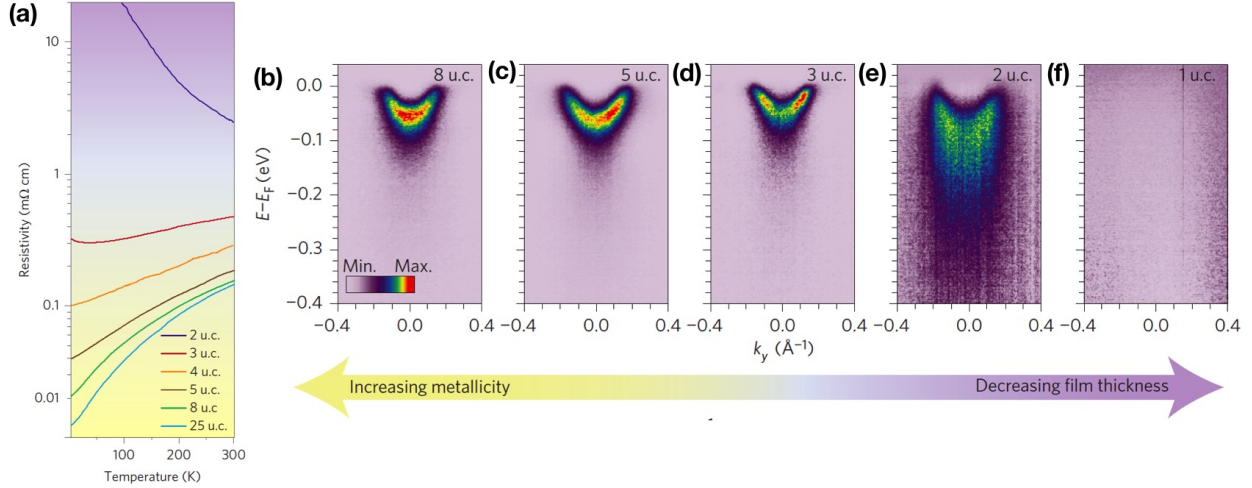


FIG. 5. (a) MITs as a function of LNO layer thickness. (b-f) The evolution of electronic structures across MIT is probed by (b-f) angle-resolved spectroscopy along $(0.5\pi/a, k_y, 0.7\pi/a)$. Abbreviations: LAO, LaAlO₃; LNO, LaNiO₃; MIT, metal-insulator transition. Reprinted by permission from Macmillan Publishers Ltd: [Nature Nanotechnology] (reference [75]), copyright (2014).

dimension [75].

2. Magnetism in Confined Architectures

Because all bulk rare earth nickelates that display a MIT also undergo magnetic transition, the observation of the insulating state in the few unit cell limit prompted several groups to investigate its spin degree of freedom. Ultrathin superlattices were initially investigated by muon spin rotation (μ SR) [99], and metallic 4-uc LNO/4-uc LAO SLs were found to remain paramagnetic down to the lowest temperatures, as for the case of bulk LNO, but antiferromagnetism was clearly detected in the insulating phase of a 2-uc LNO/2-uc LAO SL. Because μ SR cannot determine the ordering pattern, a series of LNO SLs with dielectric spacers were grown on several substrates and were investigated by resonant soft x-ray diffraction[105]. **Figure 6(a)** shows the resulting L -scans around $(1/4\ 1/4\ 1/4)_{pc}$ (where the subscripted pc denotes pseudocubic) $[(1/2\ 0\ 1/2)$ in the orthorhombic setting] with the incident photon energy tuned to the Ni L_3 edge for N uc LNO/ N uc ABO SLs with $N = 2, 3, 4$ and $ABO = \text{LAO, DyScO}_3$. The experiment clearly established the presence of bulk-like E' -type antiferromagnetic order for all of the SLs with $N=2$. The strong dependence of spin direction on underlying structure obtained from the analysis of polarization

dependence and azimuthal scans, (**Figure 6(c), (d)**) further emphasized the importance of spin-phonon coupling. Because this non-collinear antiferromagnetic structure has the same propagation wave vector as the Fermi surface nesting vector obtained from calculations and the high temperature phase is metallic (**Figure 6(b)**), this magnetic state has been interpreted as spin-density wave. The disappearance of the spin-density wave states for $N = 3, 4$ SL was attributed to the increasing three-dimensional Fermi surface that in turn suppresses the tendency for nesting together with the onset of the metallic phase. Such a nesting driven mechanism behind magnetic ordering was further corroborated by very recent ARPES measurements [106]. Similar polarization-dependent magnetic scattering experiments with azimuthal scans for thin films spanning the whole $RENiO_3$ series are clearly necessary to probe any variation in the spin orientation with the change in the Ni-O-Ni bond angles.

3. Orbital polarization

From the electronic structure standpoint, due to the strong similarity between $RENiO_3$ and high $-T_c$ cuprates (i.e. one electron *vs.* one hole on the e_g orbital), Chaloupka & Khaliullin [109] proposed, as an analog for high T_c superconductors, a single unit cell LNO layer heterostructured with a band insulator. In their model, it was assumed that tensile strain would enforce the electron in to the $d_{x^2-y^2}$ state and the insulating barrier across the interface reduce the bandwidth of the $d_{3z^2-r^2}$ band by blocking the out-of plane hopping. More recent LDA (local density approximation) + DMFT calculations corroborated the possibility of a cuprate like Fermi surface in such heterojunction [110].

This theory proposal sparked a vivid interest in orbital physics of $RENiO_3$ compounds. Apart from strain and quantum confinement, the choice of non transition metal ion X in the LNO/LaXO₃ heterostructure was shown be an important factor in controlling the degree of orbital polarization [111]. Recall that, in the bulk ligand holes are equally distributed over the six-oxygen surrounding a central Ni ion. In the LNO/LaXO₃ SL because of the strong ionic nature of X the holes initially located on the apical oxygen (i.e. Ni-O- X bond) would be redistributed back into the ab plane. This redistribution of holes would be akin to d -band filling having a strong effect on the d -orbital occupancy, altering the magnitude and even switching the sign of orbital polarization [111]. After the charge transfer physics between Ni d - states and O p states was explicitly incorporated into DFT+DMFT calculations, the resulting orbital polarization became considerably

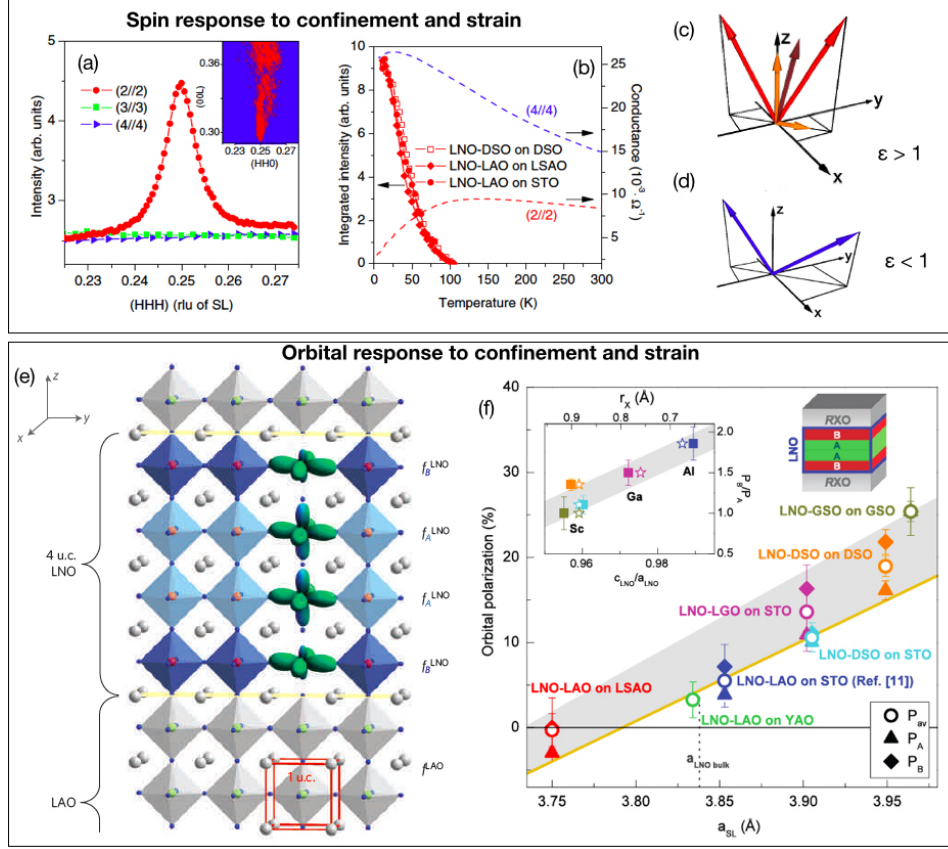


FIG. 6. (a)-(d) Effect of confinement and epitaxial strain on Ni spins, reprinted with permission from Reference [105] [A. Frano et al. Phys. Rev. Lett. **111**, 106804 (2013).] Copyright (2013) by the American Physical Society. (a) L scans around around $\mathbf{q}_0 = (1/4 \ 1/4 \ 1/4)_{pc}$ at 10 K and $E = 853.4$ eV for N u.c. LNO/ N u.c. ABO SLs (ABO= LAO, DSO). Reciprocal-space map of the scattered intensity from the $N = 2$ SL. (b) Temperature dependence of the magnetic Bragg intensity at \mathbf{q}_0 for LNO-based SLs with $N = 2$ emphasizes a paramagnetic to AFM transition. dc electrical conductance measurements for $N = 2$ and $N = 4$ SLs are also shown. (c) Spin directions of $N=2$ SL under tensile strain. Red arrows (equal moments on each site are symmetrically tilted from [001] axis by $28 \pm 2^\circ$) and orange arrows (two spin sublattices: a large moment along [001] and a small moment along [110]) show two possible arrangements. (d) The magnetic moments for $N=2$ SL under compressive strain is similar to the those of the bulk [33]. (e) Schematic structure to highlight different orbital configurations of the interfacial layer compared with the orbital configurations of the bulk-like layers, reprinted by permission from Macmillan Publishers Ltd: [Nature Materials] (reference [107]) copyright (2011). (f) Orbital polarization as a function of substrate lattice parameter for various LNO-based superlattices. Abbreviations: LAO, LaAlO₃; LNO, LaNiO₃; pc, pseudocubic; SL, superlattice; STO, SrTiO₃; DSO, DyScO₃; LSAO, LaSrAlO₄; GSO, GdScO₃; LGO, LaGaO₃; YAO, YAlO₃. Panel (f) reprinted with permission from Reference [108] [M. Wu et al., Phys. Rev. B **88**, 125124 (2013).] Copyright (2013) by the American Physical Society.

reduced [112].

The experimental work on orbital response to confinement and epitaxial strain, revealed the behavior that is significantly more complex than anticipated from the theory. For example, 1-uc LNO/1-uc LAO SLs grown under compressive strain on LAO showed equal electronic population of $d_{x^2-y^2}$ and $d_{3z^2-r^2}$ orbitals even though the orbitals an energy splitting of ~ 100 meV [113]. Disa et al[114] also recently confirmed this zero orbital polarization. In contrast, the same SL grown under tensile strain on STO showed only $\sim 5\%$ orbital polarization and most importantly no splitting between the e_g orbitals. *Ab-initio* calculations [113, 115] found that the coordination between the Al and the Ni resulted in a chemical mismatch that influenced the hole density on the apical oxygen and subsequently the Ni $d_{3z^2-r^2}$ orbital. A new approach termed orbital reflectometry (a combined analysis of XLD and resonant X-ray reflectivity) [107] applied to a 4-uc LNO/4-uc LAO superlattice (SL) on a STO substrate also detected a similar value of the orbital polarization. As illustrated in **Figure 6(c)**, the power of this method is the ability to differentiate the orbital polarization across the layers. By careful choice of spacer layers and application of high tensile strain, large orbital polarization (up to 25%) was reported for a 4-uc LNO/4-uc GdScO₃ SL [108] (**Figure 6(d)**). A very recent study of a 4-uc PrNiO₃/4-uc PrAlO₃ SL revealed the presence of smaller orbital polarization (P_{av}) of $\sim 5\%$ [116], which also decreases across the MIT. Interestingly, no significant temperature dependence of P_{av} was observed across the magnetic transition of compressively strained SLs, which had earlier been assigned as a spin density wave phase [72].

C. Interfacial charge transfer

The redistribution of charge at the interface between two dissimilar materials is one of the key concepts behind modern electronics. The difference in the chemical potential may cause charge transfer across the interface; which in-turn it can alter spin and orbital sectors, resulting in novel electronic and magnetic states emerging in complex oxide heterostructures [5–8]. For example, electronic reconstructions have been explored for LNO by forming interface with manganites [117–122] and titanates [114, 123, 124].

Although bulk CaMnO₃ (CMO) is an antiferromagnetic insulator, interfacial ferromagnetism limited within one unit cell of CMO from the interface was uncovered in N -uc CMO/ M -uc LNO superlattices when the thickness ($M \geq 4$) was sufficient to make the system metallic [120]. Because no sizable charge transfer was observed, the origin of ferromagnetism connected to the

appearance of metallicity was attributed to double exchange between Mn^{4+} and Ni^{3+} along the interface. A ferromagnetic coupling between the interfacial layers was also explored in 2-uc $\text{LaMn}^{3+}\text{O}_3/2$ uc $\text{LaNi}^{3+}\text{O}_3$ SLs, in which an electron transfer from Mn to Ni led to the formation of a $\text{Mn}^{4+} - \text{Ni}^{2+}$ pair [119]. In addition, a helical magnetic state without any spin-orbit coupling or Dzyaloshinsky-Moriya interaction, emerging from this interfacial charge transfer in LNO layers have been recently reported [125]. When prepared along the [111] direction, LNO/LaMnO₃ SLs were also displayed exchange bias, which was not seen for the [001] oriented case [118].

As a way to engineer electronic correlations, the interface between Mott insulator $\text{LaTi}^{3+}\text{O}_3$ and correlated metal LNO was recently proposed [123]. The follow-up experiments confirmed that such a heterojunction exhibits massive interfacial charge transfer from Ti to Ni sites resulting in an overall insulating ground state with a charge excitation gap of 0.2 eV between Ni d and Ti d states. The correlated gap between UHB and LHB for Ni was determined to be 1.5 eV [123, 124]. After inserting extra LaTiO_3 layers into a single unit cell LNO/LAO heterostructure, an unusually high degree of orbital polarization ($\sim 50\%$) on Ni sites has been reported and connected to the charge transfer between Ti and Ni [114, 126].

D. Geometrical Engineering

All films and heterostructures described above were synthesized along the pseudocubic [001] direction. Whereas along the $[001]_{p.c.}$ direction ABO_3 consists of alternating AO , BO_2 atomic planes, the same perovskite along the $[111]_{pc}$ direction consists of alternating $[AO_3]$ and B planes. Thus, by growing two pseudocubic unit cells of ABO_3 along $[111]_{pc}$ one can generate a new lattice with two vertically shifted triangular planes of B sites (**Figure 7(a)**). As illustrated in **Figure 7(b)**, this artificially generated buckled honeycomb lattice provides a unique opportunity to investigate physics of d electrons in graphene-like geometry [127–129]. Similarly, the dice lattice shown in **Figure 7(c)**, can be obtained by growing three unit cells along the $[1\ 1\ 1]_{pc}$ direction [130].

Due to the difference in periodic arrangements of atoms along [111] vs. [001], the theoretical calculations [128, 129, 131–133] for (111)-oriented bilayers of nickelates have predicted the realization of several exotic phases unattainable in either bulk or (001)-oriented heterojunctions. For example, the model Hamiltonian calculations in the strongly correlated limit predicted that orbital ordering wins spontaneously over the bulk-like charge ordered phase [128, 131–133], whereas in

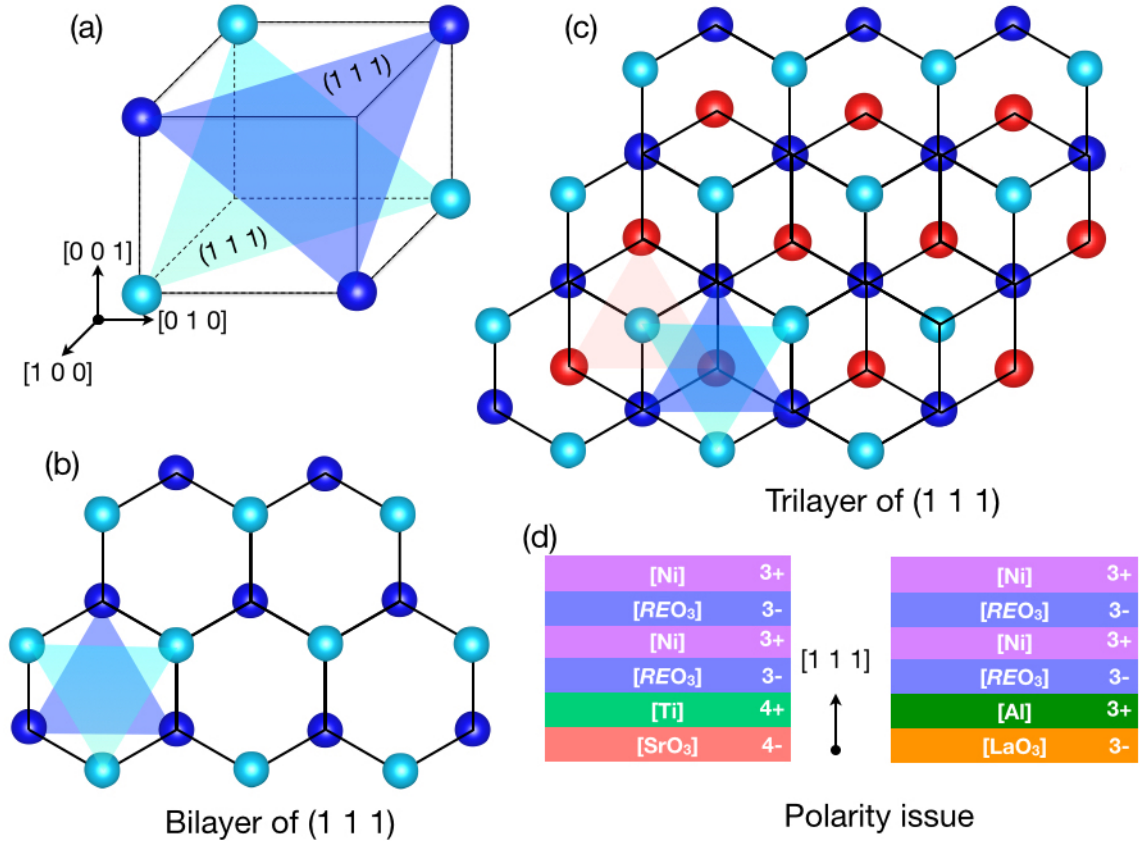


FIG. 7. (a) (111) planes of B -sites for ABO_3 perovskite structure. (b,c) Bilayer (b) and trilayer (c) of such (111) planes generate a buckled honeycomb and dice lattice, respectively. For visual clarity, A and oxygen sites are not shown. (d) Schematics of polar discontinuity (in an ionic picture and without considering any surface reconstruction) for the growth of $RENiO_3$ on STO and LAO (111) substrates. Abbreviations: LAO, $LaAlO_3$; STO, $SrTiO_3$.

the weakly correlated limit a number of topological phases (*e.g.* Dirac half-metal phase, quantum anomalous Hall insulator phase, and spin nematic phase) driven exclusively by interactions and without spin-orbit coupling were predicted [128, 129].

Because all popular perovskite substrate such as STO (LaO , $NdGaO_3$, $YAlO_3$) are polar along [111] with alternating $+4e$, $-4e$ ($+3e$, $-3e$) charges per plane, epitaxial thin film growth along this direction is rather undeveloped due to the possibility of complex structural, chemical and electronic reconstructions that act to compensate for the polarity jump. To elucidate the issue, the unit cell by unit cell growth was investigated by monitoring the growth progression with in-situ reflection high energy electron diffraction (RHEED) of LNO on STO (polar interface) and LAO (non-polar in-

terface) (111) substrates [134]. The measurements showed the presence of non-perovskite phases within the first 5 unit cells on the STO substrate; a combination of X-ray diffraction and resonant X-ray spectroscopy identified the formation of $\text{La}_2\text{Ni}_2\text{O}_5$ phase. In contrast, a stoichiometric LNO was successfully grown on a LAO (111) substrate, thus confirming that the absence of the polar mismatch at the interface is the key for the [111] oriented heterostructures [135].

Followed by the theoretical predictions [128, 129, 131–133], the behavior of d^7 Mott electrons on the honeycomb lattice was investigated by growing 2-uc NNO/4-uc LAO SL on a LAO (111) substrate. The resultant system exhibits a new ground state characterized by antiferromagnetic correlations and orbital ordering, and this lattice-geometry stabilized new ground state is unattainable in either bulk NNO or in analogous heterostructures grown along the conventional [001] direction [136]. Although design of *RE* nickelates with new lattice geometries is still in its infancy, the potential of this interesting concept for the ground state engineering was recently highlighted also by a report of markedly larger charge transfer in [*n* LNO/*n* LMO] (111) SLs with $n = 5, 7$ compared to the equivalent (001) SLs [122].

VI. THEORETICAL UNDERSTANDING

The most important task of the theory of the *RE* nickelates is to link the atomic physics of the strongly correlated Ni *d*-orbitals to the behavior of actual materials. Issues of current importance include the nature of the MIT and its connection to lattice distortions and to magnetic ordering, the degree to which orbital occupancy can be varied by strain or other external parameters, and the nature and origin of the observed magnetic states.

An important issue in the context of transition metal oxides generally and *RENiO₃* materials in particular is orbital engineering: the degree to which the electronic structure and, in particular the occupancy of different *d*-orbitals and the number of bands crossing the Fermi level can be changed by strain or by heterostructuring [7]. Following the proposal of Chaloupka and Khaliullin [109] that under appropriate circumstances LNO might exhibit a one-band Fermi surface analogous to that of the high- T_c cuprates, many groups [67, 68, 107, 108, 113, 116, 137] have investigated the degree to which orbital occupancies of *RENiO₃* materials can be manipulated. As far as is known, in bulk materials the relevant Ni *d*-orbitals are roughly equally occupied. The key finding [67, 68, 107, 108, 113, 116] is that in strained SLs a differential orbital occupancy of up to at most 25% can be achieved. Understanding the limits of orbital engineering is a second challenge

to theory.

We begin the theoretical discussion by consideration of the electronic configuration of Ni sites, which is a superposition of states with 6, 7, 8, or 9 Ni d -electrons. We can schematically write

$$|\psi_{Ni}\rangle = \alpha |d^6\rangle + \beta |d^7\rangle + \gamma |d^8\rangle + \delta |d^9\rangle \quad (2)$$

The Hund's and ligand field energies are such that the t_{2g} -symmetry d orbitals are fully filled and the relevant electronically active Ni d orbitals are the e_g states. Thus d^6 corresponds to an empty Ni e_g shell, d^7 to an e_g shell with one electron, and so forth. Although the Hund's coupling is evidently not strong enough to overcome the ligand field, it is believed to be strong enough to ensure that the dominant d^8 configuration is high-spin ($S=1$, with one electron in each e_g orbital).

The nickelates are believed to be strongly correlated materials in which interaction effects beyond DFT play a key role in the physics. As a simple example, in DFT the occupation probabilities of the different Ni valences (squares of the coefficients in Equation 2) are determined by the mean occupancy and non-interacting electron statistics; in the actual materials the mean occupancy may be different from that predicted by DFT, and the relative probabilities of different states are likely to be strongly affected by interactions. However, results of DFT calculations and their $+U$ extensions play an important role in our understanding of the materials and, at this stage, provide the only convenient mechanism for comprehensive structural relaxation, and are the starting point for beyond DFT many-body calculations.

The basic picture emerging from standard DFT calculations is that the mean Ni d -valence slightly greater than 8 [112] and that in the ideal structure two bands, of mixed Ni e_g and O_{2p} origin, cross the Fermi level (in the actual materials, monoclinic or $GdFeO_3$ -type distortions increase the unit cell so that it contains 4 Ni ions; the associated backfolding leads to multiple band crossings). Structural relaxation calculations indicate an increasing degree of $GdFeO_3$ distortion as the RE ion is changed from Nd across the series to Lu, consistent with experiment, and provide valuable information regarding rotational changes in SLs [94]. Pure DFT calculations generally predict a metallic and non-magnetic ground state in all members of the family.

The $+U$ extensions of DFT do find a charge ordered ground state for reasonable values of U [138] but greatly overestimate the critical pressure required to destroy the charge ordering.[139, 140]. Jahn-Teller effects associated with lifting the degeneracy of the two e_g states were considered by He & Millis [141] and were found to become relevant at large ($\sim 4\%$) strains. In addition, the $+U$ methodologies predict a ferromagnetic ground state, rather than the long-period E or E' state

observed experimentally. However, for a reasonable range of U , Bellaiche and co-workers [142] were able to stabilize the E' antiferromagnetic state (two inequivalent Ni atoms, one, associated with the long-bond octahedron and carrying a non-zero moment and, the other associated with the short-bond octahedron and carrying zero moment) as a metastable state. Puggioni *et al.* [143] as well as Bruno *et al.* [71] used hybrid functional methods for strained films of the nickelates to show that the experimentally observed ground state is reproduced in these calculations.

An alternative family of theoretical approaches uses model calculations based on simple physical pictures following the assumption that, in the ground state, only one valence is dominant. The Mott-Hubbard picture is based on the assumption that the relevant valence is d^7 . In this picture, the main charge transfer process involves removing an electron from one site (creating a d^6 configuration) and adding it to an adjacent site, creating a d^8 configuration, so that the key energy is $U = E(d^8) + E(d^6) - 2E(d^7)$. One expects $U > 0$, in which case the important physical effects are the Mott transition (conductivity is blocked if U is too large relative to the bandwidth) and Jahn-Teller physics associated with cubic-tetragonal distortions that lift the degeneracy of the d^7 state. Also important is the Hund's coupling, J_H , which favors high-spin configurations.

To study this situation one considers a Hubbard-like model, with two bands (representing the Ni e_g states, or, in a more sophisticated interpretation, the e_g - O_{2p} antibonding bands, and that are subject to the U , J_H and perhaps an electron-phonon interaction. Several researchers have taken this approach [95, 96, 109, 110, 138]. Mazin and co-workers [138] (using an approach based much more closely on DFT calculations) observed that at the crossover between itinerant and localized behavior (with a bandwidth comparable to the Coulomb repulsion) interesting physics can occur; in particular, if the intra-atomic exchange interaction strength J_H is large enough, it may drive charge ordering.

Hansmann and collaborators [110] studied the Mott-Hubbard picture, using a DFT+DMFT methodology in which the correlated orbitals were built from the near Fermi surface e_g -derived conduction bands. They found that for the generally accepted values of U and J the materials were near a Mott MIT. No indication of charge ordering was found. A superlattice-induced breaking of the cubic (O_h) point symmetry down to tetrahedral (T_d) was found to drive a very substantial orbital polarization, leading, for reasonable parameters, to a single-band Fermi surface.

Lee and co-workers [95, 96] addressed the weak-coupling physics of orbitally degenerate Mott-Hubbard systems by using a Hartree-Fock analysis of a two-band model with a band structure corresponding to the calculated near Fermi surface bands of LNO. A considerable degree of Fermi

surface nesting leads to a susceptibility $\chi(q)$ peaked close to the q value at which the magnetic ordering has been observed in experiments. Lee and co-workers noted that, for site-centered but not bond-centered spin-density waves, symmetry considerations imply that the magnetic ordering would lead also to a charge ordering (with an amplitude of charge order proportional to the square of the magnetic order parameter), providing a possible theoretical explanation of PrNiO₃ and NdNiO₃ for which the magnetic and charge ordering coincide. However, this reasoning cannot be extended to those nickelates for which the magnetic ordering and MIT were separated unless unreasonably large values of J_H are assumed.

If Δ is positive and reasonably large (but less than U) and β (Eq. 2) is still reasonably close to 1, one finds that the Mott-Hubbard picture provides a reasonable first-order description of the physics, with Δ playing the role of U . This picture yields, for example, the basic understanding of the high- T_c cuprates [144–146]. However in the RE nickelates, Δ may be negative, implying different physics. As noted above, DFT calculations indicate that the dominant electronic configuration is $d^8\bar{L}$ ($\gamma > \beta$) [112] and that Δ is negative. Mizokawa et al., [40] explored the potential relevance of the negative charge transfer energy situation to nickelate physics in the context of a Hartree-Fock analysis of an extended Hubbard model that also included oxygen orbitals. In this situation, holes are present on the oxygen, and a purely electronic mechanism for insulating behavior requires ordering of the oxygen holes. Ordering of oxygen holes occurred only for extremely unphysically large magnitudes of charge transfer energy ($\Delta \lesssim -7eV$), so these authors concluded that the combination of breathing-mode distortions and strong correlations on the Ni site was essential for stabilizing the insulating state.

Marianetti, one of us, and co-workers [112, 139, 140, 147] more quantitatively examined the negative charge-transfer energy scenario using a DFT+DMFT methodology in which the correlated states were taken to be atomic-like Ni states constructed from Wannier functions defined over the full energy range of the Ni-O band complex and the O states were explicitly retained in the DMFT self-consistency equation. As with all beyond-DFT approaches, the results depend to some degree on the values chosen for the interaction parameters U and J and for the double-counting correction [145, 146, 148, 149]. The important results summarized here do not depend on the precise values chosen.

The DFT+DMFT calculations lead to a mean d -occupancy slightly smaller than the ~ 8.2 value found in DFT, but still closer to 8 than to 7. One recent calculation found a mean value of ~ 7.8 , [139, 147] with $\alpha^2 = 0.24$, $\beta^2 = 0.22$, $\gamma^2 = 0.43$ and $\delta^2 = 0.11$ [150]. The dominance

of the d^8 state is characteristic of all DFT+DMFT calculations based on atomic-like Ni orbitals. Furthermore, the physically relevant values of the Hund's couplings, $J_H \sim 0.7 - 1eV$ means that the only d^8 state that occurs with appreciable probability is the high-spin d^8 in which each e_g orbital is occupied by one electron. This state is not susceptible to orbital polarization effects arising from strain or heterostructuring. In consequence, the orbital polarization is suppressed. The maximum polarization achievable under the strongest combinations of strain and heterostructuring is found to be at most $\sim 25\%$ [67, 68, 80, 107, 108, 113, 116], far too small to provide the one-band cuprate-like physics anticipated on the basis of the Mott-Hubbard-like calculations.

By solving the DFT+DMFT equations in the paramagnetic phase using the atomic positions appropriate for insulating LuNiO_3 in its ground state, Park and co-workers [147] found a novel insulating state, which may be termed either a site-selective Mott state or a hybridization wave insulator. In this state, the mean d -valences of the two structurally inequivalent Ni sites were almost the same, corresponding to approximately two electrons in the e_g orbitals. On each site, the two electrons are correlated by the Hund's coupling into an $S = 1$ state. On the long-bond site, the $S = 1$ is decoupled from the environment, so the prediction is that, for example, an NMR measurement in the paramagnetic state would reveal a freely fluctuating $S = 1$ local moment. On the other site, the $S = 1$ is strongly hybridized to the two holes on the O-sites, leading to a singlet. The DFT+DMFT calculations provide an explicit realization of this state, which is insulating. As with other DFT+ methodologies, the DFT+DMFT methodology indicates a ferrimagnetic ground state, rather than the long-period antiferromagnetic state observed experimentally. In the ferrimagnetic state, the moment size alternates: it is small on the short-bond site and large on the long-bond site. These conclusions were subsequently reproduced by Johnson et al [151] who performed exact diagonalization studies of the one- and three-dimensional Ni-O clusters.

More recently, Park et al. [139, 140] performed total energy calculations within the DFT+DMFT methodology. By examining the variation of energy along a structural path interpolating from the cubic perovskite to the experimental LuNiO_3 structure these authors showed that the DFT+DMFT methodology reproduces the salient features of the pressure- RE phase diagram of the materials, including the metallic nature of LNO and the critical pressures for the other compounds. DFT+ U methods were shown to greatly overestimate the critical pressures.

These calculations establish a reasonably consistent physical picture of the nickelates as materials with a modestly negative charge transfer energy, far from the Mott-Hubbard limit but with strong correlations, only a modest susceptibility to orbital polarization and an important coupling

between electronic behavior and the lattice. The physics involves entangled Ni- d and O $_{2p}$ states (with the entanglement crucially affected by the Hund's coupling). An interesting challenge for future research is to understand the consequences of this negative-charge-transfer physics for other aspects of the behavior of the nickelates, including the magnetic order, the quasiparticle properties of metallic states, and dynamical electron-lattice effects. In this regard, a very interesting step was taken by Subedi et al. [152] who argued that the low energy physics of the negative-charge-transfer, Ni-O-entangled state may be represented by a negative U -positive J_H Hubbard model. Further exploration of this and other theoretical approaches seems highly desirable.

VII. CONCLUDING REMARKS AND FUTURE ISSUES

With a brief introduction to the classification of electronic structure for correlated oxides, we review above the recent progress in the field of interface-controlled ground-state engineering of the $RENiO_3$ series and the simultaneous development of theoretical understanding about the origin of transitions. The possibility of realizing high-temperature superconductivity through orbital engineering was the initial motivation for studying $RENiO_3$ in ultra-thin heterostructures form, and the consequent efforts to stabilize various artificial geometries with unit cell precession have allowed for the modulation of the ground states of the bulk phase diagram. Most importantly, this heterostructuring route has also resulted in several unconventional phases such as insulating states without charge order, NFL metallic phases and antiferromagnetism in the metallic state, which are unattainable in the bulk. Here, we highlight several important issues for future consideration.

A. Exploration of crystals beyond simple perovskites

Although pushing synthesis of thin films of the highly distorted member of the series $RE = Y, Dy, Ho, \dots Lu$ is an interesting avenue of research, other geometries of Ni coordination offer interesting possibilities for tuning the physical ground states. As seen above, strained $RENiO_3$ films result in rather small orbital polarization and are limited by the ability to distort the NiO $_6$ octahedra in the highly connected perovskite network. One effective way to induce larger orbital polarization could be to move beyond simple perovskites into other classes of nickelates. One avenue involves layered nickelate phases in Ruddlesden-Popper series [153, 154] and oxygen reduced cuprate-like variants *e.g.* La $_3$ Ni $_2$ O $_6$ [155], La $_4$ Ni $_3$ O $_8$ [156, 157]. The large tetragonal distortion or absence of

the apical oxygen in these compounds gives rise to strong variations in the crystal field that can be used to tune orbital energies. In this series, thin film growth also offers opportunities to also tune orbitals via cation ordering [158]. Another option, $ANiO_2$ compounds such as $LiNiO_2$ that display interesting electronic and magnetic states [159, 160], remains largely unexplored from the perspective of epitaxial control.

B. Role of oxygen in electronic and magnetic transitions

Resonant X-ray absorption spectroscopy has firmly established the presence of holes on oxygen and the theoretical studies have also emphasized the ordering of the ligand holes in a particular fashion across the transitions. Although the checker board type charge ordering and the E' magnetic structure of the Ni sublattice have been firmly established by resonant X-ray scattering in bulk, the ligand hole ordering and magnetism associated with the oxygen sub-lattice have not been experimentally verified yet due to limitations of scattering geometry. An experimental answer to these crucial issues can be the key to disentangling the puzzle of charge and E' magnetic ordering.

C. Ground State Engineering Using External Stimuli

So far, this review focuses around metastable states created using different architectures during growth. In this section, we explore the opportunities to drive these systems non-adiabatically even further away from equilibrium via external driving forces, and we focus on two areas: optical control with visible and mid-IR sources and ionic control by applying strong electrochemical gradients. Both approaches have unique portions of phase space that can be accessed as described below.

1. Ultrafast Dynamics in Nickelate Heterostructures

Stimulating phase changes using optical pulses is a well-established way to control ground states in complex oxides [161] and offers the ability to drive a system far off the equilibrium axis as a means to trigger phase transitions or seek out wholly new emergent states. Initial work on nickelates focused on tracking the time response of the carrier dynamics [29, 162] and coherent phonon excitation to probe the nature of electron-phonon coupling [163], but recently this ap-

proach was extended using ultrafast soft X-rays to track the response of magnetism to optical excitation [164]. In NdNiO₃, the collapse of the antiferromagnetic order as probed by resonant scattering at the AFM Bragg peak revealed an ultrafast collapse of the ordering of the Ni moments, followed by much slower dynamics for the parasitic magnetism related to low-temperature ordering of the Nd moments. Direct exploration of the magnetic order gives important insight into the interaction between the MIT and magnetism. However, the recovery process is much more difficult to understand due to the high energy of optical excitation, the system equilibrates on the longer time scale of several picoseconds due to heat generated during the carrier relaxation process via electron-lattice coupling.

To circumvent this issue, researchers have been exploring mode-selective excitations that can efficiently transfer the energy in the optical excitation into the system. One very intriguing approach demonstrated recently is the direct excitation of collective modes by light in the THz-to-mid-IR regime [161, 165, 166]. This approach was first demonstrated in bulk complex oxides as a route to control the MIT by pumping specific phonon modes in the mid-IR that couple to the electronic degrees of freedom [167] and was later shown to be a route to dynamically control the superconducting phase in cuprates [168]. Caviglia et al. [84] also applied this approach to nickelate films to control the MIT. The experiment demonstrated that, by pumping a substrate phonon mode that generates an ultra fast strain wave, the system could be converted to the metallic phase [84]. By merging the mode-selective pumping with ultra fast soft X-ray scattering, Caviglia and colleagues [169] were also able to measure the propagation of the phonon from the substrate into the film by following the spatial collapse of the magnetic state. This result confirmed that the non-linear nature of the phonon excitation is a key component for triggering the transition [165]. Very recently, a DMFT theoretical framework has appeared to predict the couplings to design materials for far more efficient dynamic control [170]. In the future, this approach has the potential to offer new ways to efficiently manipulate correlated electron systems.

2. *Ionic Control*

Another new control avenue for nickelates is through the use of electric fields applied to thin-film samples to manipulate carrier doping, analogous to gate control in semiconducting devices [171]. Ionic liquids have emerged in this area as a means to apply large electric potentials through the use of a molecular electric double layer that forms on the surface of a sample. Al-

though this approach was efficiently used to control the MIT in several systems [83, 172–177], the recent picture of charge carrier doping turned out to be more related to doping via the injection of oxygen vacancies under large applied electrochemical potential gradients [178, 179]. Although the timescale of this method is much slower due to doping via ionic diffusion, this process still offers the ability to change a material’s phase through large stoichiometric changes, that were not available via gating in more conventional oxide devices [171]. Recently, in another interesting approach, the ionically gated *RE* nickelates were used to construct new classes of electronics based on neuromorphic (i.e. brain-like) principles [180, 181].

ACKNOWLEDGMENTS

The work is supported primarily by the Indo-U.S. Joint Center for Rational Control of Functional Oxides under the Indo-U.S. Science and Technology Forum. S.M. was supported by the Department of Defense-Army Research Office grant 0402-17291, and J.C. was supported by the Gordon and Betty Moore Foundation EPiQS Initiative through grant GBMF4534. Work at the Advanced Photon Source is supported by the U.S. Department of Energy, Office of Science under grant DEAC02-06CH11357. We thank S. Stemmer, S. Ramanathan, A. Georges, G. A. Fiete, and D. Khomskii for insightful comments.

-
- [1] Imada M, Fujimori A, Tokura Y. 1998. Metal-insulator transitions. *Rev. Mod. Phys.* 70:1039–1263
 - [2] Zaanen J, Sawatzky GA, Allen JW. 1985. Band gaps and electronic structure of transition-metal compounds. *Phys. Rev. Lett.* 55:418–421
 - [3] Nimkar S, Sarma DD, Krishnamurthy HR, Ramasesha S. 1993. Mean-field results of the multiple-band extended hubbard model for the square-planar CuO₂ lattice. *Phys. Rev. B* 48:7355–7363
 - [4] Zubko P, Gariglio S, Gabay M, Ghosez P, Triscone JM. 2011. Interface physics in complex oxide heterostructures. *Annual Review of Condensed Matter Physics* 2:141–165
 - [5] Hwang HY, Iwasa Y, Kawasaki M, Keimer B, Nagaosa N, Tokura Y. 2012. Emergent phenomena at oxide interfaces. *Nature Mater.* 11:103–113
 - [6] Chakhalian J, Millis AJ, Rondinelli J. 2012. Whither the oxide interface. *Nat Mater* 11:92–94

- [7] Chakhalian J, Freeland JW, Millis AJ, Panagopoulos C, Rondinelli JM. 2014. *Colloquium* : Emergent properties in plane view: Strong correlations at oxide interfaces. *Rev. Mod. Phys.* 86:1189–1202
- [8] Bhattacharya A, May SJ. 2014. Magnetic oxide heterostructures. *Annual Review of Materials Research* 44:65–90
- [9] Slater JC. 1951. Magnetic effects and the hartree-fock equation. *Physical Review* 82:538–541
- [10] Terakura K, Oguchi T, Williams AR, Kübler J. 1984. Band theory of insulating transition-metal monoxides: Band-structure calculations. *Phys. Rev. B* 30:4734–4747
- [11] Mott NF. 1949. The basis of the electron theory of metals, with special reference to the transition metals. *Proceedings of the Physical Society. Section A* 62:416
- [12] Mott NF. 1961. The transition to the metallic state. *Philosophical Magazine* 6:287—309
- [13] Hubbard J. 1963. Electron correlations in narrow energy bands. *Proceedings of the Royal Society of London A: Mathematical, Physical and Engineering Sciences* 276:238–257
- [14] Hubbard J. 1964. Electron correlations in narrow energy bands. ii. the degenerate band case. *Proceedings of the Royal Society of London A: Mathematical, Physical and Engineering Sciences* 277:237–259
- [15] Fujimori A, Minami F. 1984. Valence-band photoemission and optical absorption in nickel compounds. *Phys. Rev. B* 30:957–971
- [16] Bandyopadhyay T, Sarma DD. 1989. Calculation of coulomb interaction strengths for 3d transition metals and actinides. *Phys. Rev. B* 39:3517–3521
- [17] Mahadevan P, Shanthi N, Sarma DD. 1996. Estimates of electronic interaction parameters for LaMO_3 compounds ($M = \text{Ti-Ni}$) from *ab initio* approaches. *Phys. Rev. B* 54:11199–11206
- [18] Sarma D. 1990. Electronic structure of transition metal compounds: Photoemission experiments and model hamiltonian calculations. *J. Solid State Chem.* 88:45–52
- [19] Mizokawa T, Fujimori A, Namatame H, Akeyama K, Kosugi N. 1994. Electronic structure of the local-singlet insulator NaCuO_2 . *Phys. Rev. B* 49:7193–7204
- [20] Nimkar S, Sarma DD, Krishnamurthy HR. 1993. Electronic structure of NaCuO_2 . *Phys. Rev. B* 47:10927–10930
- [21] Sarma D, Krishnamurthy H, Nimkar S, Mitra PP, Ramasesha S, Ramakrishnan T. 1992. Electronic structure of the high t_c cuprate superconductors and related compounds. *Pramana - J. Phys.* 38:L531
- [22] Sarma D, Shanthi N, Mahadevan P. 1994. Electronic structure and the metal-insulator transition in LnNiO_3 ($\text{Ln} = \text{La, Pr, Nd, Sm and Ho}$): band structure results. *J. Phys. Condens. Matter* 6:10467

- [23] Barman SR, Chainani A, Sarma DD. 1994. Covalency-driven unusual metal-insulator transition in nickelates. *Phys. Rev. B* 49:8475–8478
- [24] Sarma DD, Shanthi N, Barman SR, Hamada N, Sawada H, Terakura K. 1995. Band theory for ground-state properties and excitation spectra of perovskite LaMO_3 ($M = \text{mn, fe, co, ni}$). *Phys. Rev. Lett.* 75:1126–1129
- [25] Medarde ML. 1997. Structural, magnetic and electronic properties of RNiO_3 perovskites ($R = \text{rare earth}$). *Journal of Physics: Condensed Matter* 9:1679
- [26] Catalan G. 2008. Progress in perovskite nickelate research. *Phase Transitions* 81:729–749
- [27] Ha SD, Jaramillo R, Silevitch DM, Schoofs F, Kerman K, et al. 2013. Hall effect measurements on epitaxial SmNiO_3 thin films and implications for antiferromagnetism. *Phys. Rev. B* 87:125150
- [28] Eguchi R, Chainani A, Taguchi M, Matsunami M, Ishida Y, et al. 2009. Fermi surfaces, electron-hole asymmetry, and correlation kink in a three-dimensional fermi liquid LaNiO_3 . *Phys. Rev. B* 79:115122
- [29] Katsufuji T, Okimoto Y, Arima T, Tokura Y, Torrance JB. 1995. Optical spectroscopy of the metal-insulator transition in NdNiO_3 . *Phys. Rev. B* 51:4830–4835
- [30] Catalan G, Bowman RM, Gregg JM. 2000. Metal-insulator transitions in NdNiO_3 thin films. *Phys. Rev. B* 62:7892–7900
- [31] Allen SJ, Hauser AJ, Mikheev E, Zhang JY, Moreno NE, et al. 2015. Gaps and pseudogaps in perovskite rare earth nickelates. *APL Materials* 3:062503
- [32] Scagnoli V, Staub U, Janousch M, Mulders AM, Shi M, et al. 2005. Charge disproportionation and search for orbital ordering in NdNiO_3 by use of resonant x-ray diffraction. *Phys. Rev. B* 72:155111
- [33] Scagnoli V, Staub U, Mulders AM, Janousch M, Meijer GI, et al. 2006. Role of magnetic and orbital ordering at the metal-insulator transition in NdNiO_3 . *Phys. Rev. B* 73:100409
- [34] García-Muñoz JL, Rodríguez-Carvajal J, Lacorre P. 1994. Neutron-diffraction study of the magnetic ordering in the insulating regime of the perovskites RNiO_3 ($R = \text{Pr and Nd}$). *Phys. Rev. B* 50:978–992
- [35] Scagnoli V, Staub U, Bodenthin Y, García-Fernández M, Mulders AM, et al. 2008. Induced non-collinear magnetic order of Nd^{3+} in NdNiO_3 observed by resonant soft x-ray diffraction. *Phys. Rev. B* 77:115138
- [36] Alonso JA, García-Muñoz JL, Fernández-Díaz MT, Aranda MAG, Martínez-Lope MJ, Casais MT. 1999. Charge disproportionation in RNiO_3 perovskites: Simultaneous metal-insulator and structural transition in YNiO_3 . *Phys. Rev. Lett.* 82:3871–3874

- [37] Vobornik I, Perfetti L, Zacchigna M, Grioni M, Margaritondo G, et al. 1999. Electronic-structure evolution through the metal-insulator transition in $R\text{NiO}_3$. *Phys. Rev. B* 60:R8426–R8429
- [38] Rodríguez-Carvajal J, Rosenkranz S, Medarde M, Lacorre P, Fernandez-Díaz MT, et al. 1998. Neutron-diffraction study of the magnetic and orbital ordering in $^{154}\text{SmNiO}_3$ and $^{153}\text{EuNiO}_3$. *Phys. Rev. B* 57:456–464
- [39] Bodenthin Y, Staub U, Piamonteze C, Garcia-Fernndez M, Martnez-Lope MJ, Alonso JA. 2011. Magnetic and electronic properties of $R\text{NiO}_3$ ($R = \text{Pr, Nd, Eu, Ho}$ and Y) perovskites studied by resonant soft x-ray magnetic powder diffraction. *Journal of Physics: Condensed Matter* 23:036002
- [40] Mizokawa T, Khomskii DI, Sawatzky GA. 2000. Spin and charge ordering in self-doped Mott insulators. *Phys. Rev. B* 61:11263
- [41] Lacorre P, Torrance J, Pannetier J, Nazzal A, Wang P, Huang T. 1991. Synthesis, crystal structure, and properties of metallic PrNiO_3 : Comparison with metallic NdNiO_3 and semiconducting SmNiO_3 . *Journal of Solid State Chemistry* 91:225 – 237
- [42] Alonso JA, Munoz A, Largeteau A, Demazeau G. 2004. Crystal growth of NdNiO_3 perovskite under high oxygen pressure. *J. Phys.: Condens. Matter* 16:S1277–S1281
- [43] Prasad KVR, Varma KBR, Raju AR, Satyalakshmi KM, Mallya RM, Hegde MS. 1993. Growth and ferroelectric properties of $\text{Bi}_2\text{VO}_{5.5}$ thin films with metallic LaNiO_3 electrodes. *Applied Physics Letters* 63:1898–1900
- [44] Yang C, Chen M, Hong T, Wu C, Wu J, Wu T. 1995. Preparation of (100)oriented metallic LaNiO_3 thin films on Si substrates by radio frequency magnetron sputtering for the growth of textured $\text{Pb}(\text{Zr}_{0.53}\text{Ti}_{0.47})\text{O}_3$. *Applied Physics Letters* 66:2643
- [45] DeNatale JF, Kobrin PH. 1996. Lattice distortion effects on electrical switching in epitaxial thin film NdNiO_3 . *J. Mater. Res.* 12:2992
- [46] Novojilov MA, Gorbenko OY, Graboy IE, Kaul AR, Zandbergen HW, et al. 2000. Perovskite rare-earth nickelates in the thin-film epitaxial state. *Applied Physics Letters* 76:2041–2043
- [47] Catalan G, Bowman RM, Gregg JM. 2000. Transport properties of NdNiO_3 thin films made by pulsed-laser deposition. *Journal of Applied Physics* 87:606–608
- [48] Son J, Moetakef P, LeBeau JM, Ouellette D, Balents L, et al. 2010. Low-dimensional mott material: Transport in ultrathin epitaxial LaNiO_3 films. *Applied Physics Letters* 96:062114
- [49] Nikolaev KR, Bhattacharya A, Kraus PA, Vas'ko VA, Cooley WK, Goldman AM. 1999. Indications of antiferromagnetic interlayer coupling in $\text{La}_{2/3}\text{Ba}_{1/3}\text{MnO}_3/\text{LaNiO}_3$ multilayers. *Applied Physics*

- [50] Kaul AR, Gorbenko OY, Kamenev AA. 2004. The role of heteroepitaxy in the development of new thin-film oxide-based functional materials. *Russ. Chem. Rev.* 73:861
- [51] Gorbenko OY, Samoilenkov S, Graboy I, Kaul A. 2002. Epitaxial stabilization of oxides in thin films. *Chemistry of materials* 14:4026–4043
- [52] Chen J, Zhou Y, Middey S, Jiang J, Chen N, et al. 2015. Self-limited kinetics of electron doping in correlated oxides. *Applied Physics Letters* 107:031905
- [53] Ha SD, Otaki M, Jaramillo R, Podpirka A, Ramanathan S. 2012. Stable metal-insulator transition in epitaxial SmNiO_3 thin films. *Journal of Solid State Chemistry* 190:233 – 237
- [54] Kareev M, Prosandeev S, Gray B, Liu J, Ryan P, et al. 2011. Sub-monolayer nucleation and growth of complex oxides at high supersaturation and rapid flux modulation. *Journal of Applied Physics* 109:114303
- [55] Feigl L, Schultz B, Ohya S, Ouellette D, Kozhanov A, Palmstram C. 2013. Structural and transport properties of epitaxial PrNiO_3 thin films grown by molecular beam epitaxy. *Journal of Crystal Growth* 366:51 – 54
- [56] Liu J, Kareev M, Gray B, Kim JW, Ryan P, et al. 2010. Strain-mediated metal-insulator transition in epitaxial ultrathin films of NdNiO_3 . *Applied Physics Letters* 96:233110
- [57] Meyers D, Moon EJ, Kareev M, Tung I, Gray BA, et al. 2013. Epitaxial stabilization of ultra-thin films of EuNiO_3 . *J. Phys. D: Appl. Phys.* 46:385303
- [58] Hauser AJ, Mikheev E, Moreno NE, Hwang J, Zhang JY, Stemmer S. 2015. Correlation between stoichiometry, strain, and metal-insulator transitions of NdNiO_3 films. *Applied Physics Letters* 106:092104
- [59] Jaramillo R, Schoofs F, Ha SD, Ramanathan S. 2013. High pressure synthesis of smnio_3 thin films and implications for thermodynamics of the nickelates. *J. Mater. Chem. C* 1:2455–2462
- [60] Bristowe N, Ghosez P, Littlewood PB, E. A. 2014. The origin of two-dimensional electron gases at oxide interfaces: insights from theory. *J. Phys.: Condens. Matter* 26:143201
- [61] Liu J, Kareev M, Prosandeev S, Gray B, Ryan P, et al. 2010. Effect of polar discontinuity on the growth of $\text{LaNiO}_3/\text{LaAlO}_3$ superlattices. *Applied Physics Letters* 96:133111
- [62] Detemple E, Ramasse QM, Sigle W, Cristiani G, Habermeier HU, et al. 2011. Polarity-driven nickel oxide precipitation in $\text{LaNiO}_3\text{-LaAlO}_3$ superlattices. *Applied Physics Letters* 99:211903

- [63] Rondinelli JM, May SJ, Freeland JW. 2012. Control of octahedral connectivity in perovskite oxide heterostructures: An emerging route to multifunctional materials discovery. *MRS Bulletin* 37:261–270
- [64] Moon EJ, Gray BA, Kareev M, Liu J, Altendorf SG, et al. 2011. Strain-dependent transport properties of the ultra-thin correlated metal, LaNiO₃. *New J. Phys.* 13:073037
- [65] Moon EJ, Rondinelli JM, Prasai N, Gray BA, Kareev M, et al. 2012. Strain-controlled band engineering and self-doping in ultrathin LaNiO₃ films. *Phys. Rev. B* 85:121106
- [66] May SJ, Kim JW, Rondinelli JM, Karapetrova E, Spaldin NA, et al. 2010. Quantifying octahedral rotations in strained perovskite oxide films. *Phys. Rev. B* 82:014110
- [67] Tung IC, Balachandran PV, Liu J, Gray BA, Karapetrova EA, et al. 2013. Connecting bulk symmetry and orbital polarization in strained RNiO₃ ultrathin films. *Phys. Rev. B* 88:205112
- [68] Chakhalian J, Rondinelli JM, Liu J, Gray BA, Kareev M, et al. 2011. Asymmetric orbital-lattice interactions in ultrathin correlated oxide films. *Phys. Rev. Lett.* 107:116805
- [69] Liu J, Kargarian M, Kareev M, Gray B, Ryan PJ, et al. 2013. Heterointerface engineered electronic and magnetic phases of NdNiO₃ thin films. *Nat Commun* 4:2714
- [70] Meyers D, Middey S, Kareev M, van Veenendaal M, Moon EJ, et al. 2013. Strain-modulated mott transition in EuNiO₃ ultrathin films. *Phys. Rev. B* 88:075116
- [71] Bruno FY, Rushchanskii KZ, Valencia S, Dumont Y, Carrétéro C, et al. 2013. Rationalizing strain engineering effects in rare-earth nickelates. *Phys. Rev. B* 88:195108
- [72] Hepting M, Minola M, Frano A, Cristiani G, Logvenov G, et al. 2014. Tunable charge and spin order in PrNiO₃ thin films and superlattices. *Phys. Rev. Lett.* 113:227206
- [73] Catalano S, Gibert M, Bisogni V, Peil OE, He F, et al. 2014. Electronic transitions in strained SmNiO₃ thin films. *APL Materials* 2:116110
- [74] Yoo HK, Hyun SI, Moreschini L, Kim HD, Chang YJ, et al. 2015. Latent instabilities in metallic LaNiO₃ films by strain control of fermi-surface topology. *Sci. Rep.* 5:8746
- [75] King PDC, Wei HI, Nie YF, Uchida M, Adamo C, et al. 2014. Atomic-scale control of competing electronic phases in ultrathin LaNiO₃. *Nat Nano* 9:443–447
- [76] Stewart MK, Liu J, Kareev M, Chakhalian J, Basov DN. 2011. Mott physics near the insulator-to-metal transition in NdNiO₃. *Phys. Rev. Lett.* 107:176401
- [77] Stewart MK, Yee CH, Liu J, Kareev M, Smith RK, et al. 2011. Optical study of strained ultrathin films of strongly correlated LaNiO₃. *Phys. Rev. B* 83:075125

- [78] Stewart MK, Brownstead D, Liu J, Kareev M, Chakhalian J, Basov DN. 2012. Heterostructuring and strain effects on the infrared optical properties of nickelates. *Phys. Rev. B* 86:205102
- [79] Tebano A, Aruta C, Sanna S, Medaglia PG, Balestrino G, et al. 2008. Evidence of orbital reconstruction at interfaces in ultrathin $\text{La}_{0.67}\text{Sr}_{0.33}\text{MnO}_3$ films. *Phys. Rev. Lett.* 100:137401
- [80] Peil OE, Ferrero M, Georges A. 2014. Orbital polarization in strained LaNiO_3 : Structural distortions and correlation effects. *Phys. Rev. B* 90:045128
- [81] Upton MH, Choi Y, Park H, Liu J, Meyers D, et al. 2015. Novel electronic behavior driving NdNiO_3 metal-insulator transition. *Phys. Rev. Lett.* 115:036401
- [82] Sarma DD, Shanthi N, Mahadevan P. 1996. Electronic excitation spectra from *ab initio* band-structure results for LaMO_3 ($M = \text{Cr, Mn, Fe, Co, Ni}$). *Phys. Rev. B* 54:1622–1628
- [83] Scherwitzl R, Zubko P, Lezama IG, Ono S, Morpurgo AF, et al. 2010. Electric-field control of the metal-insulator transition in ultrathin NdNiO_3 films. *Advanced Materials* 22:5517–5520
- [84] Caviglia AD, Scherwitzl R, Popovich P, Hu W, Bromberger H, et al. 2012. Ultrafast Strain Engineering in Complex Oxide Heterostructures. *Physical Review Letters* 108:136801
- [85] Hauser AJ, Mikheev E, Moreno NE, Cain TA, Hwang J, et al. 2013. Temperature-dependence of the hall coefficient of NdNiO_3 thin films. *Applied Physics Letters* 103:182105
- [86] Mikheev E, Hauser AJ, Himmetoglu B, Moreno NE, Janotti A, et al. 2015. Tuning bad metal and non-fermi liquid behavior in a mott material: rare earth nickelate thin films. *Science Advances* 1:e1500797
- [87] Zhou JS, Goodenough JB, Dabrowski B. 2005. Pressure-induced non-fermi-liquid behavior of PrNiO_3 . *Phys. Rev. Lett.* 94:226602
- [88] Kobayashi H, Ikeda S, Yoda Y, Hirao N, Ohishi Y, et al. 2015. Pressure-induced unusual metallic state in EuNiO_3 . *Phys. Rev. B* 91:195148
- [89] Jaramillo R, Ha SD, Silevitch DM, Ramanathan S. 2014. Origins of bad-metal conductivity and the insulator-metal transition in the rare-earth nickelates. *Nat Phys* 10:304–307
- [90] Meyers D, Liu J, Freeland JW, Middey S, Kareev M, et al. 2015. Selective interface control of order parameters in complex oxides. *condmat* 1505.07451
- [91] Staub U, Meijer GI, Fauth F, Allenspach R, Bednorz JG, et al. 2002. Direct observation of charge order in an epitaxial NdNiO_3 film. *Phys. Rev. Lett.* 88:126402
- [92] Lorenzo JE, Hodeau JL, Paolasini L, Lefloch S, Alonso JA, Demazeau G. 2005. Resonant x-ray scattering experiments on electronic orderings in NdNiO_3 single crystals. *Phys. Rev. B* 71:045128

- [93] Meyers D, Middey S, Kareev M, Liu J, Kim JW, et al. 2015. Charge order and antiferromagnetism in epitaxial ultra thin films of EuNiO_3 . *Phys. Rev. B* 92:235126
- [94] Balachandran PV, Rondinelli JM. 2013. Interplay of octahedral rotations and breathing distortions in charge-ordering perovskite oxides. *Phys. Rev. B* 88:054101
- [95] Lee SB, Chen R, Balents L. 2011. Landau theory of charge and spin ordering in the nickelates. *Phys. Rev. Lett.* 106:016405
- [96] Lee SB, Chen R, Balents L. 2011. Metal-insulator transition in a two-band model for the perovskite nickelates. *Phys. Rev. B* 84:165119
- [97] Scherwitzl R, Gariglio S, Gabay M, Zubko P, Gibert M, Triscone JM. 2011. Metal-insulator transition in ultrathin LaNiO_3 films. *Phys. Rev. Lett.* 106:246403
- [98] Liu J, Okamoto S, van Veenendaal M, Kareev M, Gray B, et al. 2011. Quantum confinement of mott electrons in ultrathin $\text{LaNiO}_3/\text{LaAlO}_3$ superlattices. *Phys. Rev. B* 83:161102
- [99] Boris AV, Matiks Y, Benckiser E, Frano A, Popovich P, et al. 2011. Dimensionality control of electronic phase transitions in nickel-oxide superlattices. *Science* 332:937–940
- [100] Sakai E, Tamamitsu M, Yoshimatsu K, Okamoto S, Horiba K, et al. 2013. Gradual localization of Ni $3d$ states in LaNiO_3 ultrathin films induced by dimensional crossover. *Phys. Rev. B* 87:075132
- [101] Kumah DP, Disa AS, Ngai JH, Chen H, Malashevich A, et al. 2014. Tuning the structure of nickelates to achieve two-dimensional electron conduction. *Advanced Materials* 26:1935–1940
- [102] Gray AX, Janotti A, Son J, LeBeau JM, Ueda S, et al. 2011. Insulating state of ultrathin epitaxial LaNiO_3 thin films detected by hard x-ray photoemission. *Phys. Rev. B* 84:075104
- [103] Kaiser AM, Gray AX, Conti G, Son J, Greer A, et al. 2011. Suppression of near-fermi level electronic states at the interface in a $\text{LaNiO}_3/(\text{SrTiO}_3)$ superlattice. *Phys. Rev. Lett.* 107:116402
- [104] Hwang J, Son J, Zhang JY, Janotti A, Van de Walle CG, Stemmer S. 2013. Structural origins of the properties of rare earth nickelate superlattices. *Phys. Rev. B* 87:060101
- [105] Frano A, Schierle E, Haverkort MW, Lu Y, Wu M, et al. 2013. Orbital control of noncollinear magnetic order in nickel oxide heterostructures. *Phys. Rev. Lett.* 111:106804
- [106] Berner G, Sing M, Pfaff F, Benckiser E, Wu M, et al. 2015. Dimensionality-tuned electronic structure of nickelate superlattices explored by soft-x-ray angle-resolved photoelectron spectroscopy. *Phys. Rev. B* 92:125130
- [107] Benckiser E, Haverkort MW, BrÄck S, Goering E, Macke S, et al. 2011. Orbital reflectometry of oxide heterostructures. *Nat Mater* 10:189–193

- [108] Wu M, Benckiser E, Haverkort MW, Frano A, Lu Y, et al. 2013. Strain and composition dependence of orbital polarization in nickel oxide superlattices. *Phys. Rev. B* 88:125124
- [109] Chaloupka Jcv, Khaliullin G. 2008. Orbital order and possible superconductivity in $\text{LaNiO}_3/\text{LaMO}_3$ superlattices. *Phys. Rev. Lett.* 100:016404
- [110] Hansmann P, Yang X, Toschi A, Khaliullin G, Andersen OK, Held K. 2009. Turning a nickelate fermi surface into a cupratelike one through heterostructuring. *Phys. Rev. Lett.* 103:016401
- [111] Han MJ, Marianetti CA, Millis AJ. 2010. Chemical control of orbital polarization in artificially structured transition-metal oxides: La_2NiXO_6 ($X = \text{B, Al, Ga, In}$) from first principles. *Phys. Rev. B* 82:134408
- [112] Han MJ, Wang X, Marianetti CA, Millis AJ. 2011. Dynamical mean-field theory of nickelate superlattices. *Phys. Rev. Lett.* 107:206804
- [113] Freeland JW, Liu J, Kareev M, Gray B, Kim JW, et al. 2011. Orbital control in strained ultra-thin $\text{LaNiO}_3/\text{LaAlO}_3$ superlattices. *Europhysics Letters* 96:57004
- [114] Disa AS, Kumah DP, Malashevich A, Chen H, Arena DA, et al. 2015. Orbital engineering in symmetry-breaking polar heterostructures. *Phys. Rev. Lett.* 114:026801
- [115] Blanca-Romero A, Pentcheva R. 2011. Confinement-induced metal-to-insulator transition in strained $\text{LaNiO}_3/\text{LaAlO}_3$ superlattices. *Phys. Rev. B* 84:195450
- [116] Wu M, Benckiser E, Audehm P, Goering E, Wochner P, et al. 2015. Orbital reflectometry of $\text{PrNiO}_3/\text{PrAlO}_3$ superlattices. *Phys. Rev. B* 91:195130
- [117] May SJ, Santos TS, Bhattacharya A. 2009. Onset of metallic behavior in strained $(\text{LaNiO}_3)_n/(\text{SrMnO}_3)_2$ superlattices. *Phys. Rev. B* 79:115127
- [118] Gibert M, Zubko P, Scherwitzl R, Añíguez J, Triscone JM. 2012. Exchange bias in LaNiO_3 - LaMnO_3 superlattices. *Nat Mater* 11:195–198
- [119] Hoffman J, Tung IC, Nelson-Cheeseman BB, Liu M, Freeland JW, Bhattacharya A. 2013. Charge transfer and interfacial magnetism in $(\text{LaNiO}_3)_n/(\text{LaMnO}_3)_2$ superlattices. *Phys. Rev. B* 88:144411
- [120] Grutter AJ, Yang H, Kirby BJ, Fitzsimmons MR, Aguiar JA, et al. 2013. Interfacial ferromagnetism in $\text{LaNiO}_3/\text{CaMnO}_3$ superlattices. *Phys. Rev. Lett.* 111:087202
- [121] Di Pietro P, Hoffman J, Bhattacharya A, Lupi S, Perucchi A. 2015. Spectral weight redistribution in $(\text{LaNiO}_3)_n/(\text{LaMnO}_3)_2$ superlattices from optical spectroscopy. *Phys. Rev. Lett.* 114:156801
- [122] Piamonteze C, Gibert M, Heidler J, Dreiser J, Rusponi S, et al. 2015. Interfacial properties of $\text{LaMnO}_3/\text{LaNiO}_3$ superlattices grown along (001) and (111) orientations. *Phys. Rev. B* 92:014426

- [123] Chen H, Millis AJ, Marianetti CA. 2013. Engineering correlation effects via artificially designed oxide superlattices. *Phys. Rev. Lett.* 111:116403
- [124] Cao Y, Liu X, Kareev M, Choudhury D, Middey S, et al. 2016. Engineered Mott ground state in a $\text{LaTiO}_{3+\delta}/\text{LaNiO}_3$ heterostructure. *Nat. Commun.* 7:10418.
- [125] Hoffman J, Kirby BJ, Kwon J, Freeland JW, Martin I, et al. 2014. Oscillatory non-collinear magnetism induced by interfacial charge transfer in metallic oxide superlattices. *arxiv* 1411.4344
- [126] Chen H, Kumah DP, Disa AS, Walker FJ, Ahn CH, Ismail-Beigi S. 2013. Modifying the electronic orbitals of nickelate heterostructures via structural distortions. *Phys. Rev. Lett.* 110:186402
- [127] Xiao D, Zhu W, Ran Y, Nagaosa N, Okamoto S. 2011. Interface engineering of quantum hall effects in digital transition metal oxide heterostructures. *Nat Commun* 2:596
- [128] Rügge A, Fiete GA. 2011. Topological insulators from complex orbital order in transition-metal oxides heterostructures. *Phys. Rev. B* 84:201103
- [129] Yang KY, Zhu W, Xiao D, Okamoto S, Wang Z, Ran Y. 2011. Possible interaction-driven topological phases in (111) bilayers of LaNiO_3 . *Phys. Rev. B* 84:201104
- [130] Wang F, Ran Y. 2011. Nearly flat band with chern number $C = 2$ on the dice lattice. *Phys. Rev. B* 84:241103
- [131] Rügge A, Mitra C, Demkov AA, Fiete GA. 2012. Electronic structure of $(\text{LaNiO}_3)_2/(\text{LaAlO}_3)_N$ heterostructures grown along [111]. *Phys. Rev. B* 85:245131
- [132] Rügge A, Mitra C, Demkov AA, Fiete GA. 2013. Lattice distortion effects on topological phases in $(\text{LaNiO}_3)_2/(\text{LaAlO}_3)_N$ heterostructures grown along the [111] direction. *Phys. Rev. B* 88:115146
- [133] Doennig D, Pickett WE, Pentcheva R. 2014. Confinement-driven transitions between topological and mott phases in $(\text{LaNiO}_3)_N/(\text{LaAlO}_3)_M$ (111) superlattices. *Phys. Rev. B* 89:121110
- [134] Middey S, Rivero P, Meyers D, Kareev M, Liu X, et al. 2014. Polarity compensation in ultra-thin films of complex oxides: The case of a perovskite nickelate. *Sci. Rep.* 4:6819
- [135] Middey S, Meyers D, Kareev M, Moon EJ, Gray BA, et al. 2012. Epitaxial growth of (111)-oriented $\text{LaAlO}_3/\text{LaNiO}_3$ ultra-thin superlattices. *Applied Physics Letters* 101:261602
- [136] Middey S, Meyers D, Doennig D, Kareev M, Liu X, et al. 2016. Mott electrons in an artificial graphenelike crystal of rare-earth nickelate. *Phys. Rev. Lett.* 116:056801.
- [137] Kinyanjui MK, Lu Y, Gauquelin N, Wu M, Frano A, et al. 2014. Lattice distortions and octahedral rotations in epitaxially strained $\text{LaNiO}_3/\text{LaAlO}_3$ superlattices. *Applied Physics Letters* 104:–

- [138] Mazin II, Khomskii DI, Lengsdorf R, Alonso JA, Marshall WG, et al. 2007. Charge ordering as alternative to Jahn-Teller distortion. *Phys. Rev. Lett.* 98:176406
- [139] Park H, Millis AJ, Marianetti CA. 2014. Total energy calculations using dft+dmft: Computing the pressure phase diagram of the rare earth nickelates. *Phys. Rev. B* 89:245133
- [140] Park H, Millis AJ, Marianetti CA. 2014. Computing total energies in complex materials using charge self-consistent DFT + DMFT. *Phys. Rev. B* 90:235103
- [141] He Z, Millis AJ. 2015. Strain control of electronic phase in rare earth nickelates. *Phys. Rev. B* 91:195138
- [142] Prosandeev S, Bellaiche L, Iniguez J. 2012. Ab initio study of the factors affecting the ground state of rare-earth nickelates. *Phys. Rev. B* 85:214431
- [143] Puggioni D, Filippetti A, Fiorentini V. 2012. Ordering and multiple phase transitions in ultrathin nickelate superlattices. *Phys. Rev. B* 86:195132
- [144] Zhang FC, Rice TM. 1988. Effective hamiltonian for the superconducting Cu oxides. *Phys. Rev. B* 37:3759–3761
- [145] de' Medici L, Wang X, Capone M, Millis AJ. 2009. Correlation strength, gaps, and particle-hole asymmetry in high- T_c cuprates: A dynamical mean field study of the three-band copper-oxide model. *Phys. Rev. B* 80:054501
- [146] Wang X, de' Medici L, Millis AJ. 2011. Role of oxygen-oxygen hopping in the three-band copper-oxide model: quasiparticle weight, metal insulator and magnetic phase boundaries, gap values and optical conductivity. *Phys. Rev. B* 83:094501
- [147] Park H, Millis AJ, Marianetti CA. 2012. Site-selective mott transition in rare-earth-element nickelates. *Phys. Rev. Lett.* 109:156402
- [148] Liechtenstein AI, Anisimov VI, Zaanen J. 1995. Density-functional theory and strong interactions: Orbital ordering in mott-hubbard insulators. *Phys. Rev. B* 52:R5467–R5470
- [149] Karolak M, Ulm G, Wehling T, Mazurenko V, Poteryaev A, Lichtenstein A. 2010. Double counting in LDA plus DMFT -the example of NiO. *Journal of Electron Spectroscopy and Related Phenomena* 181:11–15
- [150] Park H. private communication
- [151] Johnston S, Mukherjee A, Elfimov I, Berciu M, Sawatzky GA. 2014. Charge disproportionation without charge transfer in the rare-earth-element nickelates as a possible mechanism for the metal-insulator transition. *Phys. Rev. Lett.* 112:106404

- [152] Subedi A, Peil OE, Georges A. 2015. Low-energy description of the metal-insulator transition in the rare-earth nickelates. *Phys. Rev. B* 91:075128
- [153] Zhang Z, Greenblatt M, Goodenough J. 1994. Synthesis, Structure, and Properties of the Layered Perovskite $\text{La}_3\text{Ni}_2\text{O}_7-\delta$. *Journal of Solid State Chemistry* 108:402
- [154] Yoshizawa H, Kakeshita T, Kajimoto R, Tanabe T, Katsufuji T, Tokura Y. 2000. Stripe order at low temperatures in $\text{La}_{2-x}\text{Sr}_x\text{NiO}_4$ with $0.289 < x < 0.5$. *Physical Review B* 61:R854–R857
- [155] Poltavets VV, Greenblatt M, Fecher GH, Felser C. 2009. Electronic properties, band structure, and fermi surface instabilities of $\text{Ni}^{1+}/\text{Ni}^{2+}$ nickelate $\text{La}_3\text{Ni}_2\text{O}_6$, isoelectronic with superconducting cuprates. *Phys. Rev. Lett.* 102:046405
- [156] Poltavets VV, Lokshin KA, Nevidomskyy AH, Croft M, Tyson TA, et al. 2010. Bulk magnetic order in a two-dimensional $\text{Ni}^{1+}/\text{Ni}^{2+}$ (d^9/d^8) nickelate, isoelectronic with superconducting cuprates. *Phys. Rev. Lett.* 104:206403
- [157] Cheng JG, Zhou JS, Goodenough JB, Zhou HD, Matsubayashi K, et al. 2012. Pressure effect on the structural transition and suppression of the high-spin state in the triple-layer T' - $\text{La}_4\text{Ni}_3\text{O}_8$. *Phys. Rev. Lett.* 108:236403
- [158] Nelson-Cheeseman BB, Zhou H, Balachandran PV, Fabbris G, Hoffman J, et al. 2014. Polar cation ordering: A route to introducing >10% bond strain into layered oxide films. *Advanced Functional Materials* 24:6884–6891
- [159] Reynaud F, Mertz D, Celestini F, Debierre JM, Ghorayeb AM, et al. 2001. Orbital Frustration at the Origin of the Magnetic Behavior in LiNiO_2 . *Physical Review Letters* 86:3638–3641
- [160] Kang JS, Lee SS, Kim G, Lee HJ, Song HK, et al. 2007. Valence and spin states in delafossite AgNiO_2 and the frustrated jahn-teller system ANiO_2 ($A=\text{Li, Na}$). *Phys. Rev. B* 76:195122
- [161] Zhang J, Averitt RD. 2014. Dynamics and Control in Complex Transition Metal Oxides. *Annual Reviews* 44:19–43
- [162] Ruello P, Zhang S, Laffez P, Perrin B, Gusev V. 2007. Ultrafast electronic dynamics in the metal-insulator transition compound NdNiO_3 . *Physical Review B* 76:165107
- [163] Ruello P, Zhang S, Laffez P, Perrin B, Gusev V. 2009. Laser-induced coherent acoustical phonons mechanisms in the metal-insulator transition compound NdNiO_3 : Thermal and nonthermal processes. *Physical Review B* 79:094303
- [164] Caviglia AD, Rist MF, Scherwitzl R, Khanna V, Bromberger H, et al. 2013. Photoinduced melting of magnetic order in the correlated electron insulator NdNiO_3 . *Physical Review B* 88:220401

- [165] Först M, Manzoni C, Kaiser S, Tomioka Y, Tokura Y, et al. 2011. Nonlinear phononics as an ultrafast route to lattice control. *Nature Physics* 7:854
- [166] Kampfrath T, Tanaka K, Nelson KA. 2013. Resonant and nonresonant control over matter and light by intense terahertz transients. *Nature Photonics* 7:680
- [167] Rini M, Tobey R, Dean N, Itatani J, Tomioka Y, et al. 2007. Control of the electronic phase of a manganite by mode-selective vibrational excitation. *Nature* 449:72–74
- [168] Fausti D, Tobey RI, Dean N, Kaiser S, Dienst A, et al. 2011. Light-Induced Superconductivity in a Stripe-Ordered Cuprate. *Science* 331:189–191
- [169] Först M, Caviglia AD, Scherwitzl R, Mankowsky R, Zubko P, et al. 2015. Spatially resolved ultrafast magnetic dynamics initiated at a complex oxide heterointerface. *Nature Materials*
- [170] Subedi A, Cavalleri A, Georges A. 2014. Theory of nonlinear phononics for coherent light control of solids. *Physical Review B* 89:220301
- [171] Ahn CH, Di Ventra M, Eckstein JN, Frisbie CD, Gershenson ME, et al. 2006. Electrostatic modification of novel materials. *Reviews Of Modern Physics* 78:1185–1212
- [172] Ueno K, Shimotani H, Iwasa Y, Kawasaki M. 2010. Electrostatic charge accumulation versus electrochemical doping in SrTiO₃ electric double layer transistors. *Applied Physics Letters* 96:252107–252107–3
- [173] Asanuma S, Xiang PH, Yamada H, Sato H, Inoue IH, et al. 2010. Tuning of the metal-insulator transition in electrolyte-gated NdNiO₃ thin films. *Applied Physics Letters* 97:142110–142110–3
- [174] Nakano M, Shibuya K, Okuyama D, Hatano T, Ono S, et al. 2012. Collective bulk carrier delocalization driven by electrostatic surface charge accumulation. *Nature* 487:459–462
- [175] Shi J, Zhou Y, Ramanathan S. 2014. Colossal resistance switching and band gap modulation in a perovskite nickelate by electron doping. *Nature Communications* 5:4860
- [176] Ha SD, Vetter U, Shi J, Ramanathan S. 2013. Electrostatic gating of metallic and insulating phases in smnio₃ ultrathin films. *Applied Physics Letters* 102:183102
- [177] Bubel S, Hauser AJ, Glauddell AM, Mates TE, Stemmer S, Chabiny ML. 2015. The electrochemical impact on electrostatic modulation of the metal-insulator transition in nickelates. *Applied Physics Letters* 106:122102
- [178] Yang Z, Zhou Y, Ramanathan S. 2012. Studies on room-temperature electric-field effect in ionic-liquid gated VO₂ three-terminal devices. *Journal Of Applied Physics* 111:014506

- [179] Jeong J, Aetukuri N, Graf T, Schladt TD, Samant MG, Parkin SSP. 2013. Suppression of metal-insulator transition in VO₂ by electric field-induced oxygen vacancy formation. *Science* 339:1402–1405
- [180] Shi J, Ha SD, Zhou Y, Schoofs F, Ramanathan S. 2013. A correlated nickelate synaptic transistor. *Nature Communications* 4:2676
- [181] Ha S, Shi J, Meroz Y, Mahadevan L, Ramanathan S. 2014. Neuromimetic Circuits with Synaptic Devices Based on Strongly Correlated Electron Systems. *Physical Review Applied* 2:64003